Lecture note on cosmology with gravitational lensing for KEK school in 2020 January[1]

Masamune Oguri
(University of Tokyo)

version January 28, 2020

[1]If you find any typos, errors, etc., please let me know (masamune.oguri@ipmu.jp).

Contents

1 Preface

1.1 Friedmann equation

I start with a recap of the standard cosmological model without any perturbation, mainly to fix the notation that I use throughout this note. For more details on this part, please see textbooks (e.g., Dodelson, 2003; Weinberg, 2008; Matsubara, 2010). Once we accept the cosmological principle, which states that the matter distribution in the Universe is homogeneous and isotropic when viewed on a sufficiently large scale, the spacetime metric is described by the so-called Friedmann-Lemaître-Robertson-Walker (FLRW) metric

$$ds^2 = -c^2dt^2 + a^2\left[d\chi^2 + f_K^2(\chi)\left(d\theta^2 + \sin^2\theta d\phi^2\right)\right], \tag{1.1}$$

$$f_K(\chi) \coloneqq \begin{cases} (1/\sqrt{K})\sin\left(\sqrt{K}\chi\right) & (K>0), \\ \chi & (K=0), \\ (1/\sqrt{-K})\sinh\left(\sqrt{-K}\chi\right) & (K<0), \end{cases} \tag{1.2}$$

and K specifies the curvature of the space such at the Universe is closed when $K > 0$, flat when $K = 0$, and open when $K < 0$.

The evolution equation of the FLRW Universe is obtained from the Einstein equation

$$R_{\mu\nu} - \frac{1}{2}Rg_{\mu\nu} + \Lambda g_{\mu\nu} = \frac{8\pi G}{c^4}T_{\mu\nu}, \tag{1.3}$$

where $R_{\mu\nu}$ is the Ricci curvature tensor and R is the scalar curvature, both of which are computed from the metric tensor $g_{\mu\nu}$ that contains full information on the structure of spacetime. Λ is cosmological constant and $T_{\mu\nu}$ is a source term called the stress-energy tensor, which describes the energy density and momentum in spacetime. For perfect fluid, it takes the form $T^\mu{}_\nu = \mathrm{diag}(-\rho, p, p, p)$, where ρ and p are energy density and pressure of fluid, respectively. By plugging in the metric (1.1) for the Einstein equation, I obtain

$$\left(\frac{\dot{a}}{a}\right)^2 = \frac{8\pi G}{3c^2}\sum_\alpha \rho_\alpha - \frac{c^2K}{a^2} + \frac{c^2\Lambda}{3}, \tag{1.4}$$

$$\frac{\ddot{a}}{a} = -\frac{4\pi G}{3c^2}\sum_\alpha(\rho_\alpha + 3p_\alpha) + \frac{c^2\Lambda}{3}, \tag{1.5}$$

where the dot denote derivative with respect to time t and summations run over all fluid components. These equations are called Friedmann equations. Note that by moving cosmological constant to right hand side in equation (1.3), it can be regarded as one of fluid components with $\rho = c^4\Lambda/8\pi G$ and $p = -c^4\Lambda/8\pi G$.

In cosmological analysis, it is customary to define the following parameters; the Hubble parameter

$$H \coloneqq \frac{\dot{a}}{a}, \tag{1.6}$$

the critical density of the Universe

$$\rho_{\rm cr} \coloneqq \frac{3c^2H^2}{8\pi G}, \tag{1.7}$$

the density parameter

$$\Omega_\alpha \coloneqq \frac{\rho_\alpha}{\rho_{\rm cr}}, \tag{1.8}$$

and the curvature density parameter

$$\Omega_K \coloneqq -\frac{c^2K}{a^2H^2}. \tag{1.9}$$

With these parameters, the Friedmann equation (1.4) is simplified as

$$1 = \sum_\alpha \Omega_\alpha, \tag{1.10}$$

where in this expression I include both Ω_Λ and Ω_K in Ω_α.

Now I show the time evolution of the scale factor and density parameters more explicitly. I express present values of parameters defined in equations (1.6)–(1.9) by subscript 0 i.e., H_0, $\rho_{\rm cr0}$, $\Omega_{\alpha0}$, and Ω_{K0}. For the Universe that consists of the matter density $\Omega_{\rm m}$, the radiation density $\Omega_{\rm r}$, the curvature density parameter $\Omega_{\rm K}$, and cosmological constant Ω_Λ, the Friedmann equation (1.10) is expressed as

$$\frac{H^2}{H_0^2} = \Omega_{\rm r0}a^{-4} + \Omega_{\rm m0}a^{-3} + \Omega_{\rm K0}a^{-2} + \Omega_{\Lambda0}. \tag{1.11}$$

Note that the scale factor is related to redshift as

$$1 + z = \frac{1}{a}. \tag{1.12}$$

The present Universe corresponds to $z = 0$ and $a = 1$.

1.2 Distances

Adopting an observed as the origin of the spherical coordinates in the metric (1.1), χ can be seen as the comoving radial distance. From the null geodesics ($ds^2 = 0$), one can compute χ to redshift z (cosmic time t) as

$$\chi(z) = \int_{t_0}^{t} \frac{c\,dt'}{a(t')} = c\int_0^z \frac{dz'}{H(z')}. \tag{1.13}$$

Using equations (1.11) and (1.12) the Hubble parameter can expressed as a function of redshift. Ignoring the radiation component, which makes negligible contribution to distances in the late Universe, $H(z)$ is explicitly written as

$$H(z) = H_0\left[\Omega_{\rm m0}(1+z)^3 + \Omega_{\rm K0}(1+z)^2 + \Omega_{\Lambda0}\right]. \tag{1.14}$$

From equation (1.13) one can derive other distances, such as the angular diameter distance

$$D_{\rm A}(z) = \frac{f_K\left(\chi(z)\right)}{1+z}, \tag{1.15}$$

and the luminosity distance

$$D_{\rm L}(z) = (1+z)f_K\left(\chi(z)\right). \tag{1.16}$$

2 Lens equation

2.1 Metric

I now discuss light propagation in the inhomogeneous Universe, which is the main focus of this lecture. I start with assuming the following spacetime metric

$$ds^2 = -\left(1+\frac{2\Phi}{c^2}\right)c^2dt^2 + a^2\left(1-\frac{2\Psi}{c^2}\right)\left[d\chi^2 + f_K^2(\chi)\left(d\theta^2+\sin^2\theta d\phi^2\right)\right], \tag{2.1}$$

where Φ and Ψ are referred to as gravitational potential and curvature perturbation, respectively. Both Φ and Ψ are assumed to be small i.e., $|\Phi/c^2|, |\Psi/c^2| \ll 1$, which is relevant in most astronomical situations except for a few cases (e.g., light deflection very near black holes as studied in Event Horizon Telescope Collaboration et al. 2019). Note that the metric above corresponds to adopting the conformal Newtonian gauge (or longitudinal gauge), although here I do not go into detail on the gauge freedom as this lecture focuses on sub-horizon dynamics and observations.

Calculations in this metric are summarized in Appendix A. Although the Einstein equation indicates, at lease in the range of interest of this lecture, $\Phi = \Psi$ (equation A.32), here I treat Φ and Ψ separately until I derive the lens equation, in order to show their dependence on the lens equation explicitly. In fact some modified gravity theories predict $\Phi \neq \Psi$, and hence gravitational lensing provides a means of testing those modified gravity theories in combination with other cosmological observations (e.g., Jain & Khoury, 2010).

2.2 Geodesic equation

In deriving the lens equation, it is useful to treat χ (line-of-sight direction) and θ and ϕ (position on the sky) separately. For this purpose I write the metric (2.1) as

$$ds^2 = -\left(1+\frac{2\Phi}{c^2}\right)c^2dt^2 + a^2\left(1-\frac{2\Psi}{c^2}\right)\left[d\chi^2 + f_K^2(\chi)\omega_{ab}dx^adx^b\right] \qquad (a,b=2,3), \tag{2.2}$$

$$\omega_{ab}dx^adx^b \coloneqq d\theta^2+\sin^2\theta d\phi^2. \tag{2.3}$$

The light path in this metric is computed by the geodesic equation

$$\frac{d^2x^\mu}{d\lambda^2} + \Gamma^\mu{}_{\alpha\beta}\frac{dx^\alpha}{d\lambda}\frac{dx^\beta}{d\lambda} = 0, \tag{2.4}$$

where λ is an affine parameter. It is convenient to replace λ to χ for our purpose. Using the chain rule, I obtain

$$\frac{d^2x^\mu}{d\chi^2} + \Gamma^\mu{}_{\alpha\beta}\frac{dx^\alpha}{d\chi}\frac{dx^\beta}{d\chi} - \frac{d^2\lambda}{d\chi^2}\left(\frac{d\lambda}{d\chi}\right)^{-1}\frac{dx^\mu}{d\chi} = 0. \tag{2.5}$$

From the result by setting $\mu = 1$ ($x^\mu = \chi$) in equation (2.5), one can simplify equation (2.5) further as

$$\frac{d^2x^\mu}{d\chi^2} + \left(\Gamma^\mu{}_{\alpha\beta} - \Gamma^1{}_{\alpha\beta}\frac{dx^\mu}{d\chi}\right)\frac{dx^\alpha}{d\chi}\frac{dx^\beta}{d\chi} = 0. \tag{2.6}$$

Calculations of equation (2.6) requires Christoffel symbols, which are summarized in Appendix A, as well as $c\,dt/d\chi$ that is derived from the null condition

$$g_{\mu\nu}\frac{dx^\mu}{d\chi}\frac{dx^\nu}{d\chi}=0. \tag{2.7}$$

From equation (2.2),

$$\frac{c\,dt}{d\chi}=-a\left[1-\frac{\Phi}{c^2}-\frac{\Psi}{c^2}+\frac{f_K^2(\chi)}{2}\omega_{ab}\frac{dx^a}{d\chi}\frac{dx^b}{d\chi}\right], \tag{2.8}$$

up to the first order in Φ and second order in $dx^a/d\chi$. In fact, for the evaluation of equation (2.6) I need only the zero-th order result, $c\,dt/d\chi=-a$, but I show this result including perturbations as it will be used for another derivation of the lens equation discussed later. I also note that the sign of equation (2.8) is chosen as such because I consider the light path from a distant object and $\chi=0$ is chosen to be the location of an observer. By calculating the angular part ($\mu=a$) of equation (2.6), I obtain the following differential equation

$$\frac{d^2x^a}{d\chi^2}+2\frac{f_K'(\chi)}{f_K(\chi)}\frac{dx^a}{d\chi}+\frac{\omega^{ab}\left(\Phi_{,b}+\Psi_{,b}\right)}{c^2f_K^2(\chi)}=0. \tag{2.9}$$

By integrating equation (2.9) twice, I obtain

$$\begin{aligned}
x^a(\chi_{\rm s})-x^a(0) &= -\frac{1}{c^2}\int_0^{\chi_{\rm s}}d\chi'\frac{1}{f_K^2(\chi')}\int_0^{\chi'}d\chi\,\omega^{ab}\left[\Phi_{,b}(\chi,\boldsymbol{\theta}(\chi))+\Psi_{,b}(\chi,\boldsymbol{\theta}(\chi))\right]\\
&= -\frac{1}{c^2}\int_0^{\chi_{\rm s}}d\chi\,\omega^{ab}\left[\Phi_{,b}(\chi,\boldsymbol{\theta}(\chi))+\Psi_{,b}(\chi,\boldsymbol{\theta}(\chi))\right]\int_\chi^{\chi_{\rm s}}d\chi'\frac{1}{f_K^2(\chi')}\\
&= -\frac{1}{c^2}\int_0^{\chi_{\rm s}}d\chi\frac{f_K(\chi_{\rm s}-\chi)}{f_K(\chi)f_K(\chi_{\rm s})}\omega^{ab}\left[\Phi_{,b}(\chi,\boldsymbol{\theta}(\chi))+\Psi_{,b}(\chi,\boldsymbol{\theta}(\chi))\right],
\end{aligned} \tag{2.10}$$

where $\boldsymbol{\theta}=(x^2,x^3)$ specifies the angular position of light ray on the sky, which is a function of χ due to gravitational lensing deflections. Defining $(\partial_{\boldsymbol{\theta}}f)^a\coloneqq\omega^{ab}f_{,b}$, I finally obtain the lens equation for a source at the comoving radial distance $\chi=\chi_{\rm s}$ (i.e., source redshift $z_{\rm s}$ with $\chi(z_{\rm s})=\chi_{\rm s}$)

$$\boldsymbol{\theta}(\chi_{\rm s})=\boldsymbol{\theta}(0)-\frac{1}{c^2}\int_0^{\chi_{\rm s}}d\chi\frac{f_K(\chi_{\rm s}-\chi)}{f_K(\chi)f_K(\chi_{\rm s})}\partial_{\boldsymbol{\theta}}\left[\Phi(\chi,\boldsymbol{\theta}(\chi))+\Psi(\chi,\boldsymbol{\theta}(\chi))\right]. \tag{2.11}$$

This equation describes a mapping between the *source* position $\boldsymbol{\theta}(\chi_{\rm s})$ (i.e., the angular position that would be observed in absence of gravitational lensing) and the *image* position $\boldsymbol{\theta}(0)$ (i.e., the angular position that is actually observed). Figure 1 presents a schematic picture showing the source and image positions.

However, equation (2.11) contains $\boldsymbol{\theta}(\chi)$, which is known only after solving the lens equation, in the integrand, and therefore is an integral equation that is difficult to solve. A useful approximation that is commonly adopted is the Born approximation (Born, 1926) in which $\boldsymbol{\theta}(\chi)$ in the integrand is simply replaced by $\boldsymbol{\theta}(0)$ i.e.,

$$\boldsymbol{\theta}(\chi_{\rm s})=\boldsymbol{\theta}(0)-\frac{1}{c^2}\int_0^{\chi_{\rm s}}d\chi\frac{f_K(\chi_{\rm s}-\chi)}{f_K(\chi)f_K(\chi_{\rm s})}\partial_{\boldsymbol{\theta}}\left[\Phi(\chi,\boldsymbol{\theta}(0))+\Psi(\chi,\boldsymbol{\theta}(0))\right]. \tag{2.12}$$

This corresponds to the lowest order iterative approximation of the integral equation. It is shown that this approximation is sufficiently accurate for current weak lensing analysis (e.g., Krause & Hirata, 2010).

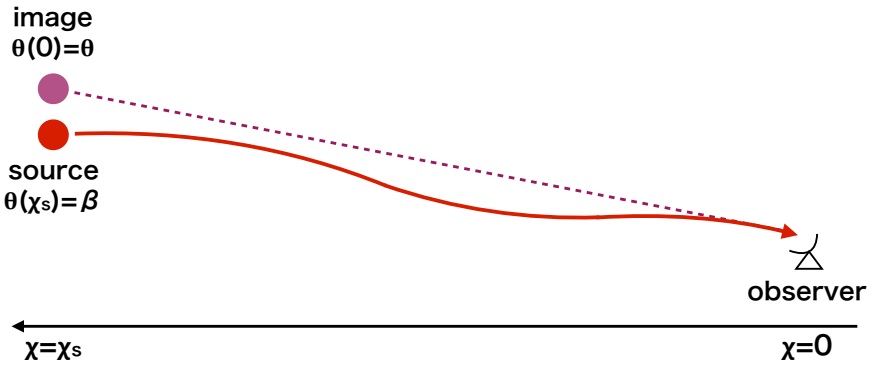

Figure 1: Schematic picture showing the source and image positions.

2.3 Fermat's principle

The derivation of the lens equation (equations 2.11 and 2.12) from the geodesic equation as shown in Section 2.2 is the standard approach. An alternative approach would be to use Fermat's principle, which states that the light ray path is determined such that its travel time T is stationary with respect to variations of the path

$$\delta T = \delta \int dt = 0. \tag{2.13}$$

I can rewrite this as

$$\delta \int d\eta = 0, \tag{2.14}$$

where $d\eta \coloneqq dt/a$ is the so-called the conformal time, because η is a monotonic function of t and all variations are performed at fixed upper limits (see Schneider, 1985). Using equation (2.8), I can rewrite this as

$$\delta \int_0^{\chi_s} d\chi \left[1 - \frac{\Phi}{c^2} - \frac{\Psi}{c^2} + \frac{f_K^2(\chi)}{2}\omega_{ab}\frac{dx^a}{d\chi}\frac{dx^b}{d\chi}\right] = 0. \tag{2.15}$$

If I define L as

$$L\left(x^a, \frac{dx^a}{d\chi}, \chi\right) \coloneqq 1 - \frac{\Phi}{c^2} - \frac{\Psi}{c^2} + \frac{f_K^2(\chi)}{2}\omega_{ab}\frac{dx^a}{d\chi}\frac{dx^b}{d\chi}, \tag{2.16}$$

equation (2.15) suggests that L satisfies the Euler-Lagrange equation

$$\frac{d}{d\chi}\left(\frac{\partial L}{\partial(dx^a/d\chi)}\right) - \frac{\partial L}{\partial x^a} = 0. \tag{2.17}$$

This leads to

$$\frac{d}{d\chi}\left[f_K^2(\chi)\omega_{ab}\frac{dx^b}{d\chi}\right] + \frac{1}{c^2}\left(\Phi_{,a} + \Psi_{,a}\right) = 0, \tag{2.18}$$

which is identical to equation (2.9). Therefore, by conducting the same calculation as done in Section 2.2 one can derive the lens equation from the Fermat's principle.

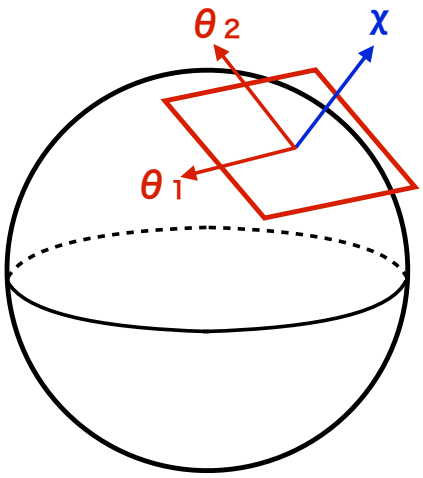

Figure 2: Locally flat coordinates on the sky.

3 Convergence and shear

3.1 Definition

In what follows, I simplify the Born-approximated lens equation (2.12) a bit further. First, since $\Phi = \Psi$ within the range of our interest, below I only use Φ. Second, although the angular coordinates defined by equation (2.3) has been assumed in the calculations above, in fact the results do not depend on the specific choice of the angular coordinates, so for simplicity I switch to locally flat coordinates (see Figure 2)

$$\omega_{ab} dx^a dx^b = \tilde{\omega}_{ab} d\tilde{x}^a d\tilde{x}^b := d\theta_1^2 + d\theta_2^2. \tag{3.1}$$

Following the convention, I also denote the image and source positions as (see also Figure 1)

$$\boldsymbol{\theta}(0) = \boldsymbol{\theta}, \tag{3.2}$$

$$\boldsymbol{\theta}(\chi_{\rm s}) = \boldsymbol{\beta}. \tag{3.3}$$

As a result, the lens equation is written as

$$\boldsymbol{\beta} = \boldsymbol{\theta} - \frac{2}{c^2} \int_0^{\chi_{\rm s}} d\chi \frac{f_K(\chi_{\rm s} - \chi)}{f_K(\chi) f_K(\chi_{\rm s})} \partial_{\boldsymbol{\theta}} \Phi(\chi, \boldsymbol{\theta}), \tag{3.4}$$

which is, again, essentially a mapping between the image position $\boldsymbol{\theta} = (\theta_1, \theta_2)$ and the source position $\boldsymbol{\beta} = (\beta_1, \beta_2)$. The second term of the right hand side of equation (3.4) is referred to as the deflection angle and is often denoted as $\boldsymbol{\alpha}$, which is a function of the image position $\boldsymbol{\theta}$ given the Born approximation. It is possible to describe the deflection angle by a gradient of the so-called lens potential ψ

$$\boldsymbol{\beta} = \boldsymbol{\theta} - \boldsymbol{\alpha}(\boldsymbol{\theta}), \tag{3.5}$$

$$\boldsymbol{\alpha}(\boldsymbol{\theta}) \coloneqq \partial_{\boldsymbol{\theta}}\psi, \tag{3.6}$$

$$\psi(\boldsymbol{\theta}) \coloneqq \frac{2}{c^2}\int_0^{\chi_{\rm s}} d\chi \frac{f_K(\chi_{\rm s}-\chi)}{f_K(\chi)f_K(\chi_{\rm s})}\Phi(\chi,\boldsymbol{\theta}). \tag{3.7}$$

Since there is no way to infer the source position $\boldsymbol{\beta}$ for a distant object at $\boldsymbol{\theta}$, one cannot directly detect gravitational lensing effects for distant objects from their positions on the sky. However, as I will show below, gravitational lensing also distorts shapes of distant objects, from which one can detect gravitational lensing effects in a statistical sense. Such distortions can be derived from equation (3.5), by considering the following Jacobi matrix

$$A \coloneqq \frac{\partial\boldsymbol{\beta}}{\partial\boldsymbol{\theta}} = I - \frac{\partial\boldsymbol{\alpha}}{\partial\boldsymbol{\theta}}, \tag{3.8}$$

where I denotes a 2×2 identity matrix. Note that A describes a mapping from an image to a source (rather than a source to an image) i.e., a shape of an image with the shape $\delta\boldsymbol{\theta}$ is mapped into a source with the shape $\delta\boldsymbol{\beta} = A\delta\boldsymbol{\theta}$. The matrix A can be decomposed into trace and traceless part as

$$A = \begin{pmatrix} 1-\kappa-\gamma_1 & -\gamma_2 \\ -\gamma_2 & 1-\kappa+\gamma_1 \end{pmatrix}, \tag{3.9}$$

where κ and γ_i are convergence and shear defined as

$$\kappa \coloneqq \frac{1}{2}\left(\psi_{,\theta_1\theta_1} + \psi_{,\theta_2\theta_2}\right), \tag{3.10}$$

$$\gamma_1 \coloneqq \frac{1}{2}\left(\psi_{,\theta_1\theta_1} - \psi_{,\theta_2\theta_2}\right), \tag{3.11}$$

$$\gamma_2 \coloneqq \psi_{,\theta_1\theta_2}. \tag{3.12}$$

Figure 3 shows how a shape of source is distorted due to κ, γ_1, and γ_2. Sometimes γ_1 and γ_2 are combined into complex shear

$$\gamma \coloneqq \gamma_1 + i\gamma_2, \tag{3.13}$$

which will be useful for various calculations as shown below.

A caveat is that γ depends on the choice of coordinates (θ_1, θ_2), which is obvious also from Figure 3. Suppose the coordinate system is rotated by an angle α i.e., $\theta' = e^{-\alpha}\theta$ in the complex plane expression, κ and γ are transformed as

$$\kappa' = \kappa, \quad \gamma' = e^{-2i\alpha}\gamma, \tag{3.14}$$

which indicates that γ is a spin-2 field (i.e., γ is not a vector).

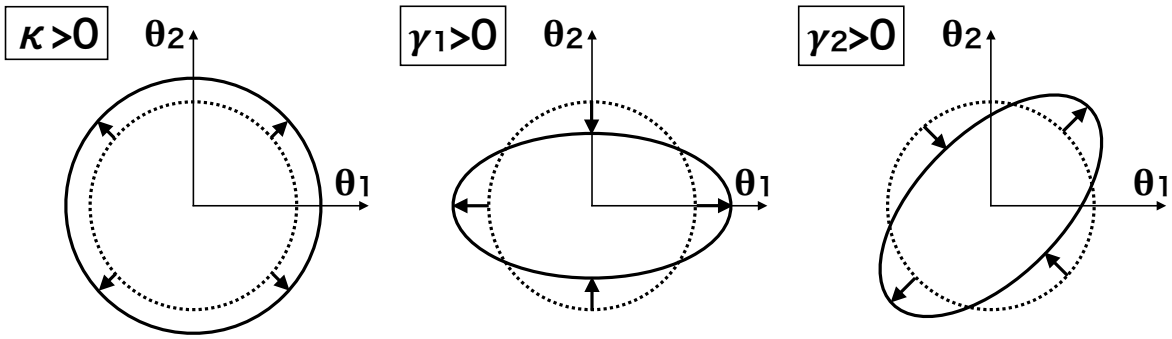

Figure 3: Distortions of galaxy shapes by gravitational lensing. Dotted circles show the original shape of a source, which is assumed to be circular symmetric. Solid lines show shapes after the gravitational lensing effect.

3.2 Measurements

When the effect of gravitational lensing is very strong, one can detect it directly from highly distorted shapes of galaxies or multiple images of sources. However, in this lecture I focus only on weak gravitational lensing where signals are weak so that they need to be detected statistically by combining many sources. Among various techniques to detect weak gravitational lensing, the most standard technique is to use shapes of source galaxies, which I will explain below.

Here I discuss a simple way to measure galaxy shapes using second moments Q_{ab} of their surface brightness distributions $I(\boldsymbol{\theta})$. For each galaxy, Q_{ab} is defined as

$$Q_{ab} \equiv \frac{\int d\boldsymbol{\theta} I(\boldsymbol{\theta})\theta_a\theta_b}{\int d\boldsymbol{\theta} I(\boldsymbol{\theta})}, \tag{3.15}$$

adopting the origin of $\boldsymbol{\theta}$ to the center of the galaxy. In a manner similar to equation (3.13), I define complex ellipticity ϵ of a galaxy as

$$\epsilon \equiv \frac{Q_{11} - Q_{22} + 2iQ_{12}}{Q_{11} + Q_{22}}. \tag{3.16}$$

Using the matrix A (equation 3.9), the corresponding second moments in the source plane $Q^{(\mathrm{s})}_{ab}$ is given by

$$Q^{(\mathrm{s})}_{ab} \equiv \frac{\int d\boldsymbol{\beta} I(\boldsymbol{\beta})\beta_a\beta_b}{\int d\boldsymbol{\beta} I(\boldsymbol{\beta})} \approx A_{ac}A_{bd}Q_{cd}, \tag{3.17}$$

where the conservation of the surface brightness distribution due to gravitational lensing ($I^{(\mathrm{s})}(\boldsymbol{\beta}) = I(\boldsymbol{\theta})$) is adopted, and adopting $\int d\boldsymbol{\beta} = \int d\boldsymbol{\theta}|\mathrm{det}A| \approx |\mathrm{det}A| \int d\boldsymbol{\theta}$ given that the size of each galaxy is sufficiently small. By a straightforward calculation, it is shown that

$$\epsilon^{(\mathrm{s})} = \frac{(1-\kappa)^2\epsilon - 2(1-\kappa)\gamma + \gamma^2\epsilon^*}{(1-\kappa)^2 + |\gamma|^2 - 2(1-\kappa)\mathrm{Re}(\gamma\epsilon^*)}. \tag{3.18}$$

This expression is simplified further by using *reduced shear* g that is defined by

$$g \coloneqq \frac{\gamma}{1-\kappa}. \tag{3.19}$$

Using reduced shear g equation (3.18) is simplified as

$$\epsilon^{(\mathrm{s})} = \frac{\epsilon - 2g + g^2\epsilon^*}{1 + |g|^2 - 2\mathrm{Re}(g\epsilon^*)}. \tag{3.20}$$

An important fact is that weak gravitational lensing in fact probes reduced shear g rather than γ, although in the weak lensing limit $\kappa \ll 1$ and hence $g \approx \gamma$ (see also Section 3.4), which can be safely assumed in most situations except for e.g., the analysis near centers of massive clusters. It is also worth noting that there is an inverse relation of equation (3.20)

$$\epsilon = \frac{\epsilon^{(\mathrm{s})} + 2g + g^2\epsilon^{(\mathrm{s})*}}{1 + |g|^2 + 2\mathrm{Re}(g\epsilon^{(\mathrm{s})*})}. \tag{3.21}$$

From equation (3.20) or (3.21), one can estimate shear for an ensemble of galaxies, assuming that galaxies are intrinsically randomly oriented i.e., $\langle\epsilon^{(\mathrm{s})}\rangle = 0$. In fact this assumption is not correct as it it known that orientations of galaxies are intrinsically aligned. While this intrinsic alignment (see e.g., Troxel & Ishak, 2015) is important for cosmic shear analysis, here I ignore it just for simplicity. Accepting $\langle\epsilon^{(\mathrm{s})}\rangle = 0$ and ignoring higher order terms,

$$\langle\epsilon\rangle \approx \langle\epsilon^{(\mathrm{s})} + 2g\rangle \approx 2g \approx 2\gamma, \tag{3.22}$$

indicating that we can estimate shear γ by averaging ellipticities of many galaxies that share the same shear value.

3.3 Connection with density fluctuations

Equation (3.10) indicates that convergence is written as the Laplacian of the lens potential in the angular coordinates, i.e., $\kappa = (1/2)\Delta_{\boldsymbol{\theta}}\psi$. Therefore, by using the Poisson equation (equation A.34) one can directly connect convergence with density fluctuations of the Universe, δ_{m} (equation A.33). Specifically, since the three-dimensional Laplace operator is written as

$${}^{(3)}\Delta\Phi = \frac{1}{f_K^2(\chi)}\frac{\partial}{\partial\chi}\left(f_K^2(\chi)\frac{\partial\Phi}{\partial\chi}\right) + \frac{1}{f_K^2(\chi)}\Delta_{\boldsymbol{\theta}}\Phi, \tag{3.23}$$

convergence is computed as

$$\begin{aligned}
\kappa(\boldsymbol{\theta}) &= \frac{1}{c^2}\int_0^{\chi_{\mathrm{s}}} d\chi \frac{f_K(\chi_{\mathrm{s}}-\chi)}{f_K(\chi)f_K(\chi_{\mathrm{s}})}\Delta_{\boldsymbol{\theta}}\Phi \\
&= \frac{1}{c^2}\int_0^{\chi_{\mathrm{s}}} d\chi \frac{f_K(\chi_{\mathrm{s}}-\chi)f_K(\chi)}{f_K(\chi_{\mathrm{s}})}\left[{}^{(3)}\Delta\Phi - \frac{1}{f_K^2(\chi)}\frac{\partial}{\partial\chi}\left(f_K^2(\chi)\frac{\partial\Phi}{\partial\chi}\right)\right] \\
&\simeq \frac{1}{c^2}\int_0^{\chi_{\mathrm{s}}} d\chi \frac{f_K(\chi_{\mathrm{s}}-\chi)f_K(\chi)}{f_K(\chi_{\mathrm{s}})}{}^{(3)}\Delta\Phi \\
&= \frac{4\pi G}{c^4}\int_0^{\chi_{\mathrm{s}}} d\chi \frac{f_K(\chi_{\mathrm{s}}-\chi)f_K(\chi)}{f_K(\chi_{\mathrm{s}})}\rho_{\mathrm{m}}a^2\delta_{\mathrm{m}}(\chi,\boldsymbol{\theta}),
\end{aligned} \tag{3.24}$$

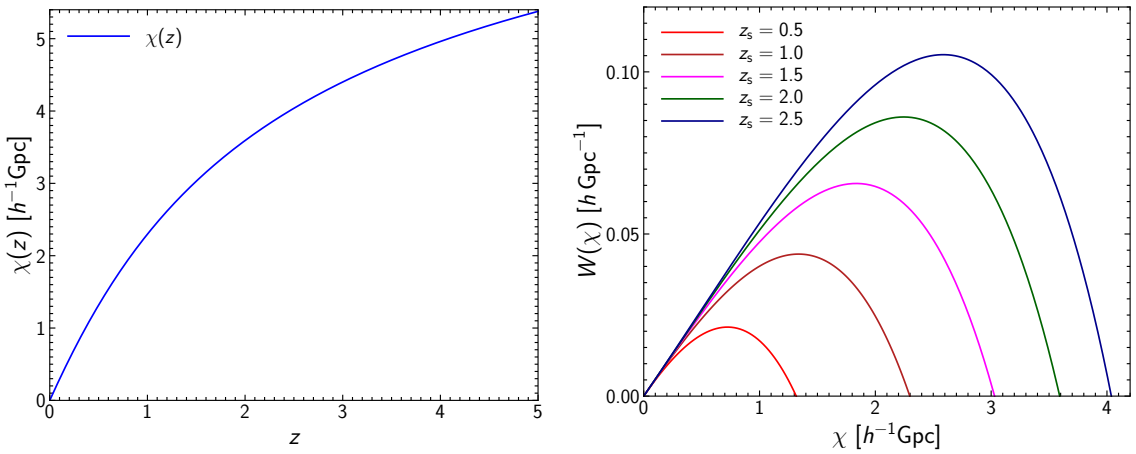

Figure 4: *Left:* The comoving radial distance χ as a function of redshift (equation 1.13). *Right:* The weight function $W(\chi)$ defined by equation (3.28) for several different source redshifts $z_{\rm s}$. Here and in what follows *Planck* 2018 best-fitting cosmological parameters (Planck Collaboration et al., 2018) are adopted.

where the approximation is based on the fact that the term proportional to Φ itself, which appears after the integration by parts, is quite small given $\mathcal{O}(10^{-5})$. Using $\Omega_{\rm m0}$ it can also be rewritten as

$$\kappa(\boldsymbol{\theta}) = \frac{3\Omega_{\rm m0}H_0^2}{2c^2}\int_0^{\chi_{\rm s}} d\chi \frac{f_K(\chi_{\rm s}-\chi)f_K(\chi)}{f_K(\chi_{\rm s})}\frac{\delta_{\rm m}(\chi,\boldsymbol{\theta})}{a}. \tag{3.25}$$

Once convergence κ is obtained from a given density field δ, the lens potential ψ from equation (3.10) using Green's function

$$\psi(\boldsymbol{\theta}) = 2\int d\boldsymbol{\theta}' G(\boldsymbol{\theta},\boldsymbol{\theta}')\kappa(\boldsymbol{\theta}') = \frac{1}{\pi}\int d\boldsymbol{\theta}' \ln\left|\boldsymbol{\theta}-\boldsymbol{\theta}'\right|\kappa(\boldsymbol{\theta}'), \tag{3.26}$$

where locally flat sky is assumed obviously and $G(\boldsymbol{x},\boldsymbol{x}') = (1/2\pi)\ln|\boldsymbol{x}-\boldsymbol{x}'|$ is Green's function for two-dimensional Laplace operator. Therefore, from a given density fluctuations, one can derive the lens potential ψ from equation (3.26), and then derive shear from equations (3.11) and (3.12).

Equations (3.24) and (3.25) indicate that κ is derived by integrating density fluctuations along the line-of-sight with a weight

$$\kappa(\boldsymbol{\theta}) = \int_0^{\chi_{\rm s}} d\chi\, W(\chi)\delta_{\rm m}(\chi,\boldsymbol{\theta}), \tag{3.27}$$

$$W(\chi) \coloneqq \frac{4\pi G}{c^4}\frac{f_K(\chi_{\rm s}-\chi)f_K(\chi)}{f_K(\chi_{\rm s})}\rho_{\rm m}a^2 = \frac{3\Omega_{\rm m0}H_0^2}{2c^2}\frac{f_K(\chi_{\rm s}-\chi)f_K(\chi)}{a\,f_K(\chi_{\rm s})}. \tag{3.28}$$

In Figure 4 we show $W(\chi)$ for several different source redshifts, along with the relation between $\chi(z)$ and z. It is found that gravitational lensing mainly probes matter fluctuations at the half way to the

source i.e., $\chi \approx \chi_{\rm s}/2$, although the weight $W(\chi)$ is sufficiently broad so that density fluctuations for a wide range of redshift contributes to the signal. It is also seen that the peak height of the weight function increases with increasing source redshift, indicating that gravitational lensing signals tend to be higher for more distant sources.

3.4 Back-of-the-envelope estimates of signal and noise

Since both κ and γ are second derivatives of the same lens potential, they are expected to be on the same order. Here I use equation (3.25) to obtain rough estimates of the amplitude of κ. Adopting crude approximations of $\delta_{\rm m}/a \approx \delta_{\rm m}(z=0)$ and $f_K(\chi_{\rm s}-\chi)f_K(\chi)/f_K(\chi_{\rm s})$ being a rectangular with the width $\chi_{\rm s}$ and the height $\chi_{\rm s}/8$, I have

$$\kappa(\boldsymbol{\theta}) \approx \frac{3\Omega_{\rm m0}}{16}\frac{\chi_{\rm s}^2}{c^2/H_0^2}\sum\frac{\Delta\chi}{\chi_{\rm s}}\delta_{\rm m}(z=0). \tag{3.29}$$

I need to specify the scale of fluctuations, because $\delta_{\rm m}$ is a random variable and its variance is a function of the smoothing scale such that density fluctuations are larger on small scales. Let's set the comoving size of fluctuations to be R, then it is natural to set $\Delta\chi = R$ and the number of independent fluctuations along the line-of-sight to be $N = \chi_{\rm s}/R$. Therefore, the root-mean square of κ for the comoving scale R, $\sigma_\kappa(R)$, is crudely estimated as

$$\sqrt{\kappa^2}(R) \approx \frac{3\Omega_{\rm m0}}{16}\frac{\chi_{\rm s}^2}{c^2/H_0^2}\frac{\sqrt{\delta_{\rm m}^2}(R)}{\sqrt{\chi_{\rm s}/R}} \approx 0.006\left(\frac{\chi_{\rm s}}{3h^{-1}{\rm Gpc}}\right)^{1.5}\left(\frac{R}{30h^{-1}{\rm Mpc}}\right)^{1/2}\sqrt{\delta_{\rm m}^2}(R, z=0). \tag{3.30}$$

The root-mean square of density fluctuations can be estimated from the nonlinear power spectrum (Takahashi et al., 2012), which is $\sqrt{\delta_{\rm m}^2} \approx 4$ at $R = 1h^{-1}$Mpc (cluster scale), ≈ 0.5 at $R = 10h^{-1}$Mpc (weakly nonlinear scale), and ≈ 0.03 at $R = 100h^{-1}$Mpc (large-scale structure scale). Inserting these numbers, I obtain

$$\sqrt{\kappa^2}(R, \chi_{\rm s} = 3h^{-1}{\rm Gpc}) \approx 0.004 \ \ (R = 1h^{-1}{\rm Mpc}), \tag{3.31}$$

$$\approx 0.002 \ \ (R = 10h^{-1}{\rm Mpc}), \tag{3.32}$$

$$\approx 0.0003 \ \ (R = 100h^{-1}{\rm Mpc}), \tag{3.33}$$

which indicates that κ (and hence $|\gamma|$) are indeed much smaller than unity, and its typical size is scale-dependent such that signals are larger on small scales.

I now discuss noise. Equation (3.22) suggests that an error σ_γ on the estimate of γ using $N_{\rm gal}$ source galaxies is

$$\sigma_\gamma = \frac{\sigma_{\epsilon/2}}{\sqrt{N_{\rm gal}}}, \tag{3.34}$$

where $\sigma_{\epsilon/2}$ is the root-mean-square of intrinsic ellipticities of galaxies ($\epsilon^{\rm (s)}/2$) and is typically $\sigma_\epsilon \approx 0.4$. The fact that σ_ϵ is much larger than expected signals shown in equations (3.31)–(3.33) immediately suggests that a large number of galaxies needs to be used in order to detect weak gravitational lensing signals. For instance, assuming $\kappa \approx |\gamma|$, it can be seen that one needs to use $N_{\rm gal} = 10^6$ galaxies in order to detect the signal at $R = 10h^{-1}$Mpc (equation 3.32) with signal-to-noise ratio of $S/N = 5$. Modern surveys use $N_{\rm gal} = 10^7$ or more galaxies to measure weak gravitational lensing signals at various scales (e.g., Hikage et al., 2019).

4 Cosmic shear power spectrum

4.1 Fourier transform and E/B decomposition

One of the most popular ways to extract cosmological weak gravitational lensing signals is to measure two-point correlation functions, or their counterparts in Fourier space, power spectra. Since calculations are more convenient in Fourier space, here I introduce convergence and shear in Fourier space and discuss their properties.

I again adopt locally flat coordinates, and use the following convention to perform Fourier transform

$$\kappa(\boldsymbol{\theta}) = \int \frac{d\boldsymbol{\ell}}{(2\pi)^2}\,\tilde{\kappa}(\boldsymbol{\ell})e^{i\boldsymbol{\ell}\cdot\boldsymbol{\theta}}, \tag{4.1}$$

$$\tilde{\kappa}(\boldsymbol{\ell}) = \int d\boldsymbol{\theta}\,\kappa(\boldsymbol{\theta})e^{-i\boldsymbol{\ell}\cdot\boldsymbol{\theta}}. \tag{4.2}$$

Similarly I denote Fourier transform of complex shear as $\tilde{\gamma}$.

As shown in equation (3.14) shear is not invariant under coordinate rotation. This coordinate rotation also changes $\tilde{\gamma}$ as $\tilde{\gamma}' = e^{-2i\alpha}\tilde{\gamma}$. From $\tilde{\gamma}$, I define new fields $\tilde{\gamma}_{\rm E}$ and $\tilde{\gamma}_{\rm B}$ that are designed to be invariant under coordinate rotation

$$\tilde{\gamma}_{\rm E} \coloneqq \cos(2\phi_{\boldsymbol{\ell}})\,\tilde{\gamma}_1 + \sin(2\phi_{\boldsymbol{\ell}})\,\tilde{\gamma}_2, \tag{4.3}$$

$$\tilde{\gamma}_{\rm B} \coloneqq -\sin(2\phi_{\boldsymbol{\ell}})\,\tilde{\gamma}_1 + \cos(2\phi_{\boldsymbol{\ell}})\,\tilde{\gamma}_2, \tag{4.4}$$

where $\phi_{\boldsymbol{\ell}}$ is a polar angle in Fourier space i.e., $(\ell_1,\,\ell_2)$=$(|\boldsymbol{\ell}|\cos\phi_{\boldsymbol{\ell}},\,|\boldsymbol{\ell}|\sin\phi_{\boldsymbol{\ell}})$. They satisfy

$$\tilde{\gamma}_{\rm E} + i\tilde{\gamma}_{\rm B} = e^{-2i\phi_{\boldsymbol{\ell}}}\tilde{\gamma}. \tag{4.5}$$

Under coordinated rotation with angle α, $\tilde{\gamma} \to e^{-2i\alpha}\tilde{\gamma}$ and $\phi_{\boldsymbol{\ell}} \to \phi_{\boldsymbol{\ell}} - \alpha$, and hence the right hand side of equation (4.5) does not change.

The physical meaning of $\tilde{\gamma}_{\rm E}$ and $\tilde{\gamma}_{\rm B}$ becomes clearer once they are transformed to real space. From equation (4.5), I can obtain their expressions in real space as

$$\begin{aligned}\gamma_{\rm E}(\boldsymbol{\theta}) + i\gamma_{\rm B}(\boldsymbol{\theta}) &= \int \frac{d\boldsymbol{\ell}}{(2\pi)^2}\,e^{i\boldsymbol{\ell}\cdot\boldsymbol{\theta}} \int d\boldsymbol{\theta}'\,\gamma(\boldsymbol{\theta}')e^{-i\boldsymbol{\ell}\cdot\boldsymbol{\theta}'} \int d\boldsymbol{\theta}''\,D(\boldsymbol{\theta}'')e^{-i\boldsymbol{\ell}\cdot\boldsymbol{\theta}''} \\ &= \int d\boldsymbol{\theta}'\gamma(\boldsymbol{\theta}')D(\boldsymbol{\theta}-\boldsymbol{\theta}'),\end{aligned} \tag{4.6}$$

where I used a useful formula for Dirac delta function $\delta^{\rm D}(\boldsymbol{\theta})$

$$\int \frac{d\boldsymbol{\ell}}{(2\pi)^2}\,e^{i\boldsymbol{\ell}\cdot\boldsymbol{\theta}} = \delta^{\rm D}(\boldsymbol{\theta}), \tag{4.7}$$

and $D(\boldsymbol{\theta})$ is Fourier transform of $e^{-2i\phi_{\boldsymbol{\ell}}}$ and is given by

$$D(\boldsymbol{\theta}) = -\frac{1}{\pi}\frac{e^{-2i\phi_{\boldsymbol{\theta}}}}{|\boldsymbol{\theta}|^2} = -\frac{1}{\pi}\frac{\theta_1^2 - \theta_2^2 - 2i\theta_1\theta_2}{|\boldsymbol{\theta}|^4}, \tag{4.8}$$

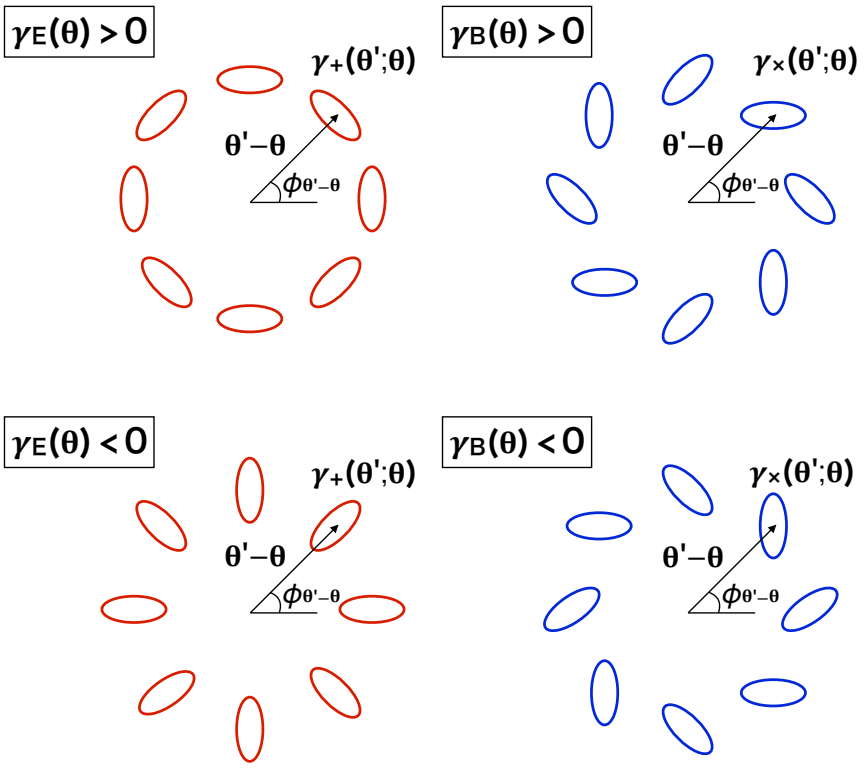

Figure 5: Meaning of E-mode and B-mode shear (see equation 4.9). E-mode shear $\gamma_{\rm E}(\boldsymbol{\theta})$ is essentially summation of tangential shear $\gamma_+(\boldsymbol{\theta}';\,\boldsymbol{\theta})$ (equation 4.10) around $\boldsymbol{\theta}$, and B-mode shear $\gamma_{\rm E}(\boldsymbol{\theta})$ is summation of cross shear $\gamma_\times(\boldsymbol{\theta}';\,\boldsymbol{\theta})$ (equation 4.11) around $\boldsymbol{\theta}$.

with $\phi_{\boldsymbol{\theta}}$ being a polar angle in real space i.e., $(\theta_1,\,\theta_2)=(|\boldsymbol{\theta}|\cos\phi_{\boldsymbol{\theta}},\,|\boldsymbol{\theta}|\sin\phi_{\boldsymbol{\theta}})$. Inserting this expression to equation (4.6), I obtain

$$\gamma_{\rm E}(\boldsymbol{\theta})+i\gamma_{\rm B}(\boldsymbol{\theta})=\frac{1}{\pi}\int d\boldsymbol{\theta}'\,\frac{\gamma_+(\boldsymbol{\theta}';\,\boldsymbol{\theta})}{\left|\boldsymbol{\theta}-\boldsymbol{\theta}'\right|^2}+i\frac{1}{\pi}\int d\boldsymbol{\theta}'\,\frac{\gamma_\times(\boldsymbol{\theta}';\,\boldsymbol{\theta})}{\left|\boldsymbol{\theta}-\boldsymbol{\theta}'\right|^2}, \tag{4.9}$$

where

$$\gamma_+(\boldsymbol{\theta}';\,\boldsymbol{\theta}) \;\coloneqq\; -{\rm Re}\left[\gamma(\boldsymbol{\theta}')\,e^{-2i\phi_{\boldsymbol{\theta}'-\boldsymbol{\theta}}}\right]=-\gamma_1(\boldsymbol{\theta}')\cos(2\phi_{\boldsymbol{\theta}'-\boldsymbol{\theta}})-\gamma_2(\boldsymbol{\theta}')\sin(2\phi_{\boldsymbol{\theta}'-\boldsymbol{\theta}}), \tag{4.10}$$

$$\gamma_\times(\boldsymbol{\theta}';\,\boldsymbol{\theta}) \;\coloneqq\; -{\rm Im}\left[\gamma(\boldsymbol{\theta}')\,e^{-2i\phi_{\boldsymbol{\theta}'-\boldsymbol{\theta}}}\right]=\gamma_1(\boldsymbol{\theta}')\sin(2\phi_{\boldsymbol{\theta}'-\boldsymbol{\theta}})-\gamma_2(\boldsymbol{\theta}')\cos(2\phi_{\boldsymbol{\theta}'-\boldsymbol{\theta}}). \tag{4.11}$$

From the definition of shear, it is easily found that $\gamma_+(\boldsymbol{\theta}';\,\boldsymbol{\theta})$ and $\gamma_\times(\boldsymbol{\theta}';\,\boldsymbol{\theta})$ represents tangential shear and its 45° rotated version (sometimes referred to as cross shear) around $\boldsymbol{\theta}$, respectively. Thus in analogy to electromagnetics, $\gamma_{\rm E}$ and $\gamma_{\rm B}$ is E-mode and B-mode shear, respectively. Figure 5 gives an explanation of E-mode and B-mode shear.

Now let's see the relation of $\gamma_{\rm E}$ and $\gamma_{\rm B}$ with convergence. From equations (3.10)–(3.12) in Fourier space convergence is related with shear as

$$\tilde{\kappa} = e^{-2i\phi_{\boldsymbol{\ell}}}\tilde{\gamma}. \tag{4.12}$$

This indicates

$$\gamma_{\rm E} = \kappa, \qquad \gamma_{\rm B} = 0, \tag{4.13}$$

i.e., gravitational lensing produces only E-mode shear. Note that equation (4.13) is exactly true only under Born approximation. Higher order effects produce small B-mode, which is ~ 3 orders of magnitude smaller than E-mode and hence can be ignored in most cases (e.g., Krause & Hirata, 2010).

4.2 Definition of power spectrum

The power spectrum, which is Fourier transform of two-point correlation function, plays a central role in cosmology. For instance, in the three-dimensional space the two-point correlation function of density fluctuations is usually defined as

$$\xi_{\rm m}(r) \coloneqq \langle \delta_{\rm m}(\boldsymbol{r}')\delta_{\rm m}(\boldsymbol{r}'+\boldsymbol{r})\rangle, \tag{4.14}$$

where $r = |\boldsymbol{r}|$ is the separation and $\langle\ldots\rangle$ denotes ensemble average. From this, the correlation of density fluctuations in Fourier space is computed as

$$\langle\tilde{\delta}(\boldsymbol{k})\tilde{\delta}(\boldsymbol{k}')\rangle = \int d\boldsymbol{r}'\, e^{-i\boldsymbol{k}\cdot\boldsymbol{r}'}\int d\boldsymbol{r}''\, e^{-i\boldsymbol{k}'\cdot\boldsymbol{r}''}\langle\delta_{\rm m}(\boldsymbol{r}')\delta_{\rm m}(\boldsymbol{r}'')\rangle = (2\pi)^3\delta^{\rm D}(\boldsymbol{k}+\boldsymbol{k}')\int d\boldsymbol{r}\, e^{-i\boldsymbol{k}\cdot\boldsymbol{r}}\xi_{\rm m}(r), \tag{4.15}$$

where I used

$$\int \frac{d\boldsymbol{r}}{(2\pi)^3}\, e^{i\boldsymbol{k}\cdot\boldsymbol{r}} = \delta^{\rm D}(\boldsymbol{k}). \tag{4.16}$$

The matter power spectrum $P_{\rm m}(k)$ as a function of wavenumber $k \coloneqq |\boldsymbol{k}|$ is defined by

$$\langle\tilde{\delta}(\boldsymbol{k})\tilde{\delta}(\boldsymbol{k}')\rangle \coloneqq (2\pi)^3\delta^{\rm D}(\boldsymbol{k}+\boldsymbol{k}')P_{\rm m}(k), \tag{4.17}$$

which satisfies

$$P_{\rm m}(k) = \int d\boldsymbol{r}\, e^{-i\boldsymbol{k}\cdot\boldsymbol{r}}\xi_{\rm m}(r) = 4\pi\int r^2 dr\, \frac{\sin(kr)}{kr}\xi_{\rm m}(r), \tag{4.18}$$

indicating that the power spectrum is given by Fourier transform of two-point correlation function (known as the Wiener–Khinchin theorem). The two-point correlation function and the power spectrum depends only on norms of $\boldsymbol{r}$ and $\boldsymbol{k}$, respectively, because the Universe is on average isotropic.

Power spectra of convergence and shear can be defined in a similar fashion. Specifically, I define angular power spectra C_ℓ as a function of $\ell \coloneqq |\boldsymbol{\ell}|$ as

$$\langle\tilde{\kappa}(\boldsymbol{\ell})\tilde{\kappa}(\boldsymbol{\ell}')\rangle \coloneqq (2\pi)^2\delta^{\rm D}(\boldsymbol{\ell}+\boldsymbol{\ell}')C_\ell^{\kappa\kappa}, \tag{4.19}$$

and

$$C_\ell^{\kappa\kappa} = \int d\boldsymbol{\theta}\, e^{-i\boldsymbol{\theta}\cdot\boldsymbol{\ell}}\omega^{\kappa\kappa}(\theta) = 2\pi\int\theta d\theta\, J_0(\ell\theta)\,\omega^{\kappa\kappa}(\theta), \tag{4.20}$$

where $\omega^{\kappa\kappa}(\theta)$ is angular two-point correlation function as a function of $\theta \coloneqq |\boldsymbol{\theta}|$ defined by

$$\omega^{\kappa\kappa}(\theta) \coloneqq \langle \kappa(\boldsymbol{\theta}')\kappa(\boldsymbol{\theta}'+\boldsymbol{\theta})\rangle, \tag{4.21}$$

and $J_0(x)$ is the zeroth order Bessel function. In deriving the equation above, I used an integral formula of Bessel function $J_n(x)$

$$J_n(x) = \frac{1}{2\pi i^n}\int_0^{2\pi} e^{in\phi + ix\cos\phi} d\phi. \tag{4.22}$$

In a manner similar to above, I can define power spectrum and correlation functions for various shear components. A caveat is that γ_1 and γ_2 are coordinate-dependent, and therefore their correlation functions and power spectra depend on directions of $\boldsymbol{\theta}$ and $\boldsymbol{\ell}$, respectively. Specifically I write

$$\langle \tilde{\gamma}_i(\boldsymbol{\ell})\tilde{\gamma}_j(\boldsymbol{\ell}')\rangle \coloneqq (2\pi)^2\delta^{\rm D}(\boldsymbol{\ell}+\boldsymbol{\ell}')C_{\boldsymbol{\ell}}^{\gamma_i\gamma_j}, \tag{4.23}$$

$$C_{\boldsymbol{\ell}}^{\gamma_i\gamma_j} = \int d\boldsymbol{\theta}\, e^{-i\boldsymbol{\theta}\cdot\boldsymbol{\ell}}\omega^{\gamma_i\gamma_j}(\boldsymbol{\theta}), \tag{4.24}$$

$$\omega^{\gamma_i\gamma_j}(\boldsymbol{\theta}) \coloneqq \langle \gamma_i(\boldsymbol{\theta}')\gamma_i(\boldsymbol{\theta}'+\boldsymbol{\theta})\rangle, \tag{4.25}$$

where γ_i and γ_j are γ_1, γ_2, γ_+, $\gamma_\times$, $\gamma_{\rm E}$, $\gamma_{\rm B}$, as well as complex representation of shear γ (equation 3.13). From equation (4.13), it is found $C_\ell^{\kappa\kappa} = C_\ell^{\gamma_{\rm E}\gamma_{\rm E}}$ and $C_\ell^{\gamma_{\rm B}\gamma_{\rm B}} = 0$ under Born approximation.

4.3 Connection with two-point correlation function

While there are several different approaches to study correlations of shear in real space, here I focus on the following two correlation functions (e.g., Kaiser, 1992)

$$\xi_\pm(\theta) \coloneqq \omega^{\gamma_+\gamma_+}(\theta) \pm \omega^{\gamma_\times\gamma_\times}(\theta), \tag{4.26}$$

where $\omega^{\gamma_+\gamma_+}(\theta)$ and $\omega^{\gamma_\times\gamma_\times}(\theta)$ are defined by

$$\omega^{\gamma_+\gamma_+}(\theta) \coloneqq \langle \gamma_+(\boldsymbol{\theta}';\boldsymbol{\theta}'+\boldsymbol{\theta})\gamma_+(\boldsymbol{\theta}'+\boldsymbol{\theta};\boldsymbol{\theta}')\rangle, \tag{4.27}$$

$$\omega^{\gamma_\times\gamma_\times}(\theta) \coloneqq \langle \gamma_\times(\boldsymbol{\theta}';\boldsymbol{\theta}'+\boldsymbol{\theta})\gamma_\times(\boldsymbol{\theta}'+\boldsymbol{\theta};\boldsymbol{\theta}')\rangle, \tag{4.28}$$

where γ_+ and $\gamma_\times$ has been defined in equations (4.10) and (4.11). Note that these are coordinate-independent correlation functions, and also that $\omega^{\gamma_+\gamma_\times}(\theta) = 0$ given that the Universe is statistically invariant under a parity transformation. From the definitions of γ_+ and $\gamma_\times$,

$$\omega^{\gamma_+\gamma_+}(\theta) = \cos^2(2\phi_{\boldsymbol{\theta}})\,\omega^{\gamma_1\gamma_1}(\boldsymbol{\theta}) + \sin^2(2\phi_{\boldsymbol{\theta}})\,\omega^{\gamma_2\gamma_2}(\boldsymbol{\theta}) + 2\sin(2\phi_{\boldsymbol{\theta}})\cos(2\phi_{\boldsymbol{\theta}})\,\omega^{\gamma_1\gamma_2}(\boldsymbol{\theta}), \tag{4.29}$$

$$\omega^{\gamma_\times\gamma_\times}(\theta) = \sin^2(2\phi_{\boldsymbol{\theta}})\,\omega^{\gamma_1\gamma_1}(\boldsymbol{\theta}) + \cos^2(2\phi_{\boldsymbol{\theta}})\,\omega^{\gamma_2\gamma_2}(\boldsymbol{\theta}) - 2\sin(2\phi_{\boldsymbol{\theta}})\cos(2\phi_{\boldsymbol{\theta}})\,\omega^{\gamma_1\gamma_2}(\boldsymbol{\theta}), \tag{4.30}$$

and hence $\xi_\pm(\theta)$ are expressed as

$$\xi_+(\theta) = \omega^{\gamma_1\gamma_1}(\boldsymbol{\theta}) + \omega^{\gamma_2\gamma_2}(\boldsymbol{\theta}) = \omega^{\gamma\gamma^*}(\boldsymbol{\theta}), \tag{4.31}$$

$$\xi_-(\theta) = \cos(4\phi_{\boldsymbol{\theta}})\left[\omega^{\gamma_1\gamma_1}(\boldsymbol{\theta}) - \omega^{\gamma_2\gamma_2}(\boldsymbol{\theta})\right] + 2\sin(4\phi_{\boldsymbol{\theta}})\,\omega^{\gamma_1\gamma_2}(\boldsymbol{\theta}) = \mathrm{Re}\left[e^{-4i\phi_{\boldsymbol{\theta}}}\omega^{\gamma\gamma}(\boldsymbol{\theta})\right]. \tag{4.32}$$

On the other hand, from equations (4.3) and (4.4) I also have

$$C_{\boldsymbol{\ell}}^{\gamma\gamma^*} = C_\ell^{\gamma_{\rm E}\gamma_{\rm E}} + C_\ell^{\gamma_{\rm B}\gamma_{\rm B}}, \tag{4.33}$$

$$C_{\boldsymbol{\ell}}^{\gamma\gamma} = e^{4i\phi_{\boldsymbol{\ell}}}\left(C_\ell^{\gamma_{\rm E}\gamma_{\rm E}} - C_\ell^{\gamma_{\rm B}\gamma_{\rm B}}\right), \tag{4.34}$$

where I used the fact that $C^{\gamma_{\rm E}\gamma_{\rm B}} = 0$ again due to the invariance under a parity transformation. Combining the equations above, I finally obtain

$$\xi_+(\theta) = \int \frac{d\boldsymbol{\ell}}{(2\pi)^2}\left(C_\ell^{\gamma_{\rm E}\gamma_{\rm E}} + C_\ell^{\gamma_{\rm B}\gamma_{\rm B}}\right)e^{i\boldsymbol{\ell}\cdot\boldsymbol{\theta}} = \int_0^\infty \frac{\ell d\ell}{2\pi}\left(C_\ell^{\gamma_{\rm E}\gamma_{\rm E}} + C_\ell^{\gamma_{\rm B}\gamma_{\rm B}}\right)J_0(\ell\theta), \tag{4.35}$$

$$\xi_-(\theta) = \mathrm{Re}\left[e^{-4i\phi_{\boldsymbol{\theta}}}\int \frac{d\boldsymbol{\ell}}{(2\pi)^2}e^{4i\phi_{\boldsymbol{\ell}}}\left(C_\ell^{\gamma_{\rm E}\gamma_{\rm E}} - C_\ell^{\gamma_{\rm B}\gamma_{\rm B}}\right)e^{i\boldsymbol{\ell}\cdot\boldsymbol{\theta}}\right] = \int_0^\infty \frac{\ell d\ell}{2\pi}\left(C_\ell^{\gamma_{\rm E}\gamma_{\rm E}} - C_\ell^{\gamma_{\rm B}\gamma_{\rm B}}\right)J_4(\ell\theta), \tag{4.36}$$

where an integral formula for the Bessel function (equation 4.22) has been used. This result indicates that two-point correlation functions of shear are indeed related with angular power spectrum of shear.

4.4 Calculation of power spectrum

I now evaluate cosmic shear power spectrum $C_\ell^{\kappa\kappa} = C_\ell^{\gamma_{\rm E}\gamma_{\rm E}}$. From equations (3.27) and (4.2), Fourier transform of convergence is given by

$$\begin{aligned}
\tilde{\kappa}(\boldsymbol{\ell}) &= \int d\boldsymbol{\theta}\, e^{-i\boldsymbol{\ell}\cdot\boldsymbol{\theta}}\int_0^{\chi_{\rm s}} d\chi\, W(\chi)\delta_{\rm m}(\chi,\boldsymbol{\theta}) \\
&= \int d\boldsymbol{\theta}\, e^{-i\boldsymbol{\ell}\cdot\boldsymbol{\theta}}\int_0^{\chi_{\rm s}} d\chi\, W(\chi)\int \frac{d\boldsymbol{k}}{(2\pi)^3}\tilde{\delta}_{\rm m}(\boldsymbol{k})e^{i\boldsymbol{k}\cdot\boldsymbol{r}} \\
&= \int d\boldsymbol{\theta}\, e^{-i\boldsymbol{\ell}\cdot\boldsymbol{\theta}}\int_0^{\chi_{\rm s}} d\chi\, W(\chi)\int \frac{dk_\parallel}{2\pi}\frac{d\boldsymbol{k}_\perp}{(2\pi)^2}\tilde{\delta}_{\rm m}(k_\parallel,\boldsymbol{k}_\perp)e^{i\left\{k_\parallel\chi + f_K(\chi)\boldsymbol{k}_\perp\cdot\boldsymbol{\theta}\right\}} \\
&= \int_0^{\chi_{\rm s}} d\chi\,\frac{W(\chi)}{f_K^2(\chi)}\int \frac{dk_\parallel}{2\pi}\tilde{\delta}_{\rm m}\left(k_\parallel,\frac{\boldsymbol{\ell}}{f_K(\chi)}\right)e^{ik_\parallel\chi},
\end{aligned} \tag{4.37}$$

where $k_\parallel$ and $\boldsymbol{k}_\perp$ are wavenumbers that are parallel and perpendicular to the line-of-sight direction, respectively. From this expression, correlation of convergence in Fourier space is

$$\begin{aligned}\langle\tilde{\kappa}(\boldsymbol{\ell})\tilde{\kappa}(\boldsymbol{\ell}')\rangle &= \int_0^{\chi_\mathrm{s}} d\chi\,\frac{W(\chi)}{f_K^2(\chi)}\int_0^{\chi_\mathrm{s}} d\chi'\,\frac{W(\chi')}{f_K^2(\chi')}\int\frac{dk_\parallel}{2\pi}\int\frac{dk'_\parallel}{2\pi}e^{i(k_\parallel\chi+k'_\parallel\chi')} \\ &\quad\times\left\langle\tilde{\delta}_\mathrm{m}\left(k_\parallel,\frac{\boldsymbol{\ell}}{f_K(\chi)}\right)\tilde{\delta}_\mathrm{m}\left(k'_\parallel,\frac{\boldsymbol{\ell}'}{f_K(\chi')}\right)\right\rangle \\ &= \int_0^{\chi_\mathrm{s}} d\chi\,\frac{W(\chi)}{f_K^2(\chi)}\int_0^{\chi_\mathrm{s}} d\chi'\,\frac{W(\chi')}{f_K^2(\chi')}\int\frac{dk_\parallel}{2\pi}e^{ik_\parallel(\chi-\chi')}P_\mathrm{m}\left(\sqrt{k_\parallel^2+\frac{\ell^2}{f_K^2(\chi)}}\right) \\ &\quad\times(2\pi)^2\delta^\mathrm{D}\left(\frac{\boldsymbol{\ell}}{f_K(\chi)}+\frac{\boldsymbol{\ell}'}{f_K(\chi')}\right). \end{aligned} \tag{4.38}$$

I now make the following additional approximation. When $k_\parallel \gg \ell/f_K(\chi)$, due to the rapid oscillation by $e^{ik_\parallel(\chi-\chi')}$ it vanishes after integrations over χ, given that $W(\chi)$ is sufficiently broad (see Figure 4). Hence I consider only modes with $k_\parallel \ll \ell/f_K(\chi)$, which results in

$$\int\frac{dk_\parallel}{2\pi}e^{ik_\parallel(\chi-\chi')}P_\mathrm{m}\left(\sqrt{k_\parallel^2+\frac{\ell^2}{f_K^2(\chi)}}\right)\approx\delta^\mathrm{D}(\chi-\chi')P_\mathrm{m}\left(\frac{\ell}{f_K(\chi)}\right), \tag{4.39}$$

which is called the Limber approximation (Limber, 1954). By performing the integration over χ', I now have a simplified expression for the correlation

$$\langle\tilde{\kappa}(\boldsymbol{\ell})\tilde{\kappa}(\boldsymbol{\ell}')\rangle=(2\pi)^2\delta^\mathrm{D}\left(\boldsymbol{\ell}+\boldsymbol{\ell}'\right)\int_0^{\chi_\mathrm{s}} d\chi\frac{W^2(\chi)}{f_K^2(\chi)}P_\mathrm{m}\left(\frac{\ell}{f_K(\chi)};\chi\right), \tag{4.40}$$

where I added the argument χ in the matter power spectrum to make it explicit that the matter power spectrum at the redshift corresponding to χ should be used there. From the definition of angular power spectrum (equation 4.19), I finally obtain cosmic shear power spectrum

$$C_\ell^{\kappa\kappa}=\int_0^{\chi_\mathrm{s}} d\chi\frac{W^2(\chi)}{f_K^2(\chi)}P_\mathrm{m}\left(\frac{\ell}{f_K(\chi)};\chi\right), \tag{4.41}$$

where the weight function $W(\chi)$ has been defined in equation (3.28). While equation (4.41) is sufficiently accurate and is used for cosmological analysis, it should be kept in mind that it is built on various approximations such as Born approximation, locally flat sky approximation, and Limber approximation. For instance, it has been shown that the following slightly modified version

$$C_\ell^{\kappa\kappa}=\int_0^{\chi_\mathrm{s}} d\chi\frac{W^2(\chi)}{f_K^2(\chi)}P_\mathrm{m}\left(\frac{\ell+1/2}{f_K(\chi)};\chi\right), \tag{4.42}$$

better reproduces the full calculation result at low ℓ (Loverde & Afshordi, 2008).

4.5 Shot noise

In practice the power spectrum has to be estimated from a discrete galaxy sample, which has an impact of the measurement of the power spectrum. As discussed in Section 3.2, shapes of galaxies provide noisy measurements of weak gravitational lensing shear. Given equation (3.22), for each galaxy labeled by i located at $\boldsymbol{\theta}_i$, I define an estimator of shear as

$$\gamma_i^{\rm obs} \coloneqq \frac{\epsilon_i}{2} \approx \frac{\epsilon_i^{\rm (s)}}{2} + \gamma(\boldsymbol{\theta}_i), \tag{4.43}$$

where ϵ_i and $\epsilon_i^{\rm (s)}$ denote observed and intrinsic ellipticities of the galaxy, respectively. From a discrete galaxy sample, I construct observed shear field using a cell model (see e.g., Mo et al., 2010). I divide the survey region into small cells with areas of $\Delta\Omega$. Each cell is sufficient small such that it contains at most one galaxy. The estimator of the shear field is written as

$$\gamma^{\rm obs}(\boldsymbol{\theta}) \coloneqq \frac{1}{\bar{n}} \sum_i N_i \gamma_i^{\rm obs} \delta^{\rm D}(\boldsymbol{\theta} - \boldsymbol{\theta}_i), \tag{4.44}$$

where $\bar{n}$ is (projected) angular number density of galaxies, $N_i = 0$ or 1 is an occupation number at i-th cell, and the summation runs over the cells. From $\langle N_i \gamma_i^{\rm obs}\rangle = \langle N_i\rangle\langle\gamma_i^{\rm obs}\rangle = \bar{n}\Delta\Omega\langle\gamma_i^{\rm obs}\rangle$, from which one can show $\langle\gamma_{\rm obs}(\boldsymbol{\theta})\rangle = \langle\gamma(\boldsymbol{\theta})\rangle$. Using equation (4.2), its Fourier transform is computed as

$$\tilde{\gamma}^{\rm obs}(\boldsymbol{\ell}) = \frac{1}{\bar{n}} \sum_i N_i \gamma_i^{\rm obs} e^{-i\boldsymbol{\ell}\cdot\boldsymbol{\theta}_i}. \tag{4.45}$$

Equation (4.12) suggests that the correlation E-mode shear $\tilde{\gamma}_{\rm E}^{\rm obs}(\boldsymbol{\ell})$ (see equation 4.3) is computed as

$$\langle \tilde{\gamma}_{\rm E}^{\rm obs}(\boldsymbol{\ell}) \tilde{\gamma}_{\rm E}^{\rm obs}(\boldsymbol{\ell}')\rangle = \frac{1}{\bar{n}^2} \sum_{i,j} \langle N_i N_j \gamma_{{\rm E},i}^{\rm obs} \gamma_{{\rm E},j}^{\rm obs}\rangle e^{-i(\boldsymbol{\ell}\cdot\boldsymbol{\theta}_i + \boldsymbol{\ell}'\cdot\boldsymbol{\theta}_j)}. \tag{4.46}$$

and

$$\begin{aligned}
\langle N_i N_j \gamma_{{\rm E},i}^{\rm obs} \gamma_{{\rm E},j}^{\rm obs}\rangle &= \left\langle N_i N_j \frac{\epsilon_{{\rm E},i}^{\rm (s)}}{2} \frac{\epsilon_{{\rm E},j}^{\rm (s)}}{2} \right\rangle + \langle N_i N_j \gamma_{\rm E}(\boldsymbol{\theta}_i)\gamma_{\rm E}(\boldsymbol{\theta}_j)\rangle \\
&= \bar{n}\Delta\Omega\delta_{ij} \frac{\sigma_{\epsilon/2}^2}{2} + (\bar{n}\Delta\Omega)^2 \langle \gamma_{\rm E}(\boldsymbol{\theta}_i)\gamma_{\rm E}(\boldsymbol{\theta}_j)\rangle,
\end{aligned} \tag{4.47}$$

where $\sigma_{\epsilon/2} (\approx 0.4)$ is the root-mean-square of intrinsic ellipticities and a factor $1/2$ originates from the fact that random intrinsic ellipticities contribute to both E-mode and B-mode equally (i.e., $\sigma_{\epsilon_{\rm E}/2}^2 = \sigma_{\epsilon_{\rm B}/2}^2 = \sigma_{\epsilon/2}^2/2$). From this expression, equation (4.46) reduces to

$$\begin{aligned}
\langle \tilde{\gamma}_{\rm E}^{\rm obs}(\boldsymbol{\ell}) \tilde{\gamma}_{\rm E}^{\rm obs}(\boldsymbol{\ell}')\rangle &= \frac{1}{\bar{n}} \sum_i \Delta\Omega \frac{\sigma_{\epsilon/2}^2}{2} e^{-i(\boldsymbol{\ell}+\boldsymbol{\ell}')\cdot\boldsymbol{\theta}_i} + \sum_{i,j} (\Delta\Omega)^2 \langle \gamma_{\rm E}(\boldsymbol{\theta}_i)\gamma_{\rm E}(\boldsymbol{\theta}_j)\rangle e^{-i(\boldsymbol{\ell}\cdot\boldsymbol{\theta}_i + \boldsymbol{\ell}'\cdot\boldsymbol{\theta}_j)} \\
&\approx \frac{\sigma_{\epsilon/2}^2}{2\bar{n}} \int d\boldsymbol{\theta}_i e^{-i(\boldsymbol{\ell}+\boldsymbol{\ell}')\cdot\boldsymbol{\theta}_i} + \int d\boldsymbol{\theta}_i \int d\boldsymbol{\theta}'_j\, \omega^{\gamma_{\rm E}\gamma_{\rm E}}(\theta'_j)\, e^{-i(\boldsymbol{\ell}+\boldsymbol{\ell}')\cdot\boldsymbol{\theta}_i - i\boldsymbol{\ell}'\cdot\boldsymbol{\theta}'_j} \\
&= (2\pi)^2 \delta^{\rm D}(\boldsymbol{\ell}+\boldsymbol{\ell}') \left(\frac{\sigma_{\epsilon/2}^2}{2\bar{n}} + C_\ell^{\gamma_{\rm E}\gamma_{\rm E}} \right)
\end{aligned} \tag{4.48}$$

Therefore, an observed cosmic shear power spectrum $C_\ell^{\gamma_{\rm E}\gamma_{\rm E},{\rm obs}}$ from a discrete galaxy sample becomes

$$C_\ell^{\gamma_{\rm E}\gamma_{\rm E},{\rm obs}} = C_\ell^{\gamma_{\rm E}\gamma_{\rm E}} + \frac{\sigma^2_{\epsilon/2}}{2\bar{n}}. \tag{4.49}$$

The second term that is inversely proportional to the angular number density of galaxies is called the shot noise. Although the shot noise term can be estimated from the observation and therefore one can obtain $C_\ell^{\gamma_{\rm E}\gamma_{\rm E}}$ from the observed data, it is still very important as it contributes to the noise as I will see below.

4.6 Covariance

Since the measurement error of power spectrum depends on the survey area, Fourier transform should also be performed in a limited sky area. Let's assume that the survey region is a rectangular with the length Θ. Adopting the size of a cell in $\boldsymbol{\ell}$ space as $\Delta\ell = 2\pi/\Theta$ (i.e., $\Delta\Omega = (2\pi/\Theta)^2$), equation (4.1) is modified as

$$\kappa(\boldsymbol{\theta}) = \sum_i \frac{(\Delta\ell)^2}{(2\pi)^2}\,\tilde{\kappa}(\boldsymbol{\ell}_i)e^{i\boldsymbol{\ell}_i\cdot\boldsymbol{\theta}} = \frac{1}{\Omega_{\rm s}}\sum_i \tilde{\kappa}(\boldsymbol{\ell}_i)e^{i\boldsymbol{\ell}_i\cdot\boldsymbol{\theta}}, \tag{4.50}$$

where $\Omega_{\rm s} = \Theta^2$ is the total survey area. Using this discretized description in $\boldsymbol{\ell}$ space, E-mode power spectrum in i-th ℓ bin defined by $\ell_{i,\rm min} < \ell < \ell_{i,\rm max}$ is estimated as

$$\hat{C}_{\ell,i}^{\gamma_{\rm E}\gamma_{\rm E},{\rm obs}} \coloneqq \frac{1}{\Omega_{\rm s}N_{{\rm mode},i}}\sum_{\boldsymbol{\ell}\in i}\tilde{\gamma}_{\rm E}^{\rm obs}(\boldsymbol{\ell})\tilde{\gamma}_{\rm E}^{\rm obs}(-\boldsymbol{\ell}), \tag{4.51}$$

where

$$N_{{\rm mode},i} \coloneqq \frac{\pi\left(\ell^2_{i,\rm max} - \ell^2_{i,\rm min}\right)}{\Delta\ell^2} = f_{\rm sky}\left(\ell^2_{i,\rm max} - \ell^2_{i,\rm min}\right), \tag{4.52}$$

is the number of modes in the bin and $f_{\rm sky} \coloneqq \Omega_{\rm s}/(4\pi)$. Using a discrete version of the definition of power spectrum

$$\langle\tilde{\gamma}_{\rm E}^{\rm obs}(\boldsymbol{\ell}_i)\tilde{\gamma}_{\rm E}^{\rm obs}(\boldsymbol{\ell}_j)\rangle = \Omega_{\rm s}\delta_{\boldsymbol{\ell}_i+\boldsymbol{\ell}_j}C_{\ell,i}^{\gamma_{\rm E}\gamma_{\rm E},{\rm obs}}, \tag{4.53}$$

with $\delta_{\boldsymbol{\ell}_i+\boldsymbol{\ell}_j} = 1$ only when $\boldsymbol{\ell}_i + \boldsymbol{\ell}_j = 0$, it is shown that $\langle\hat{C}_{\ell,i}^{\gamma_{\rm E}\gamma_{\rm E},{\rm obs}}\rangle = C_{\ell,i}^{\gamma_{\rm E}\gamma_{\rm E},{\rm obs}}$.

I now derive covariance between i-th and j-th ℓ bins. It is defined by

$$\begin{aligned}\left[{\rm Cov}(\hat{C}_\ell^{\gamma_{\rm E}\gamma_{\rm E}})\right]_{ij} &\coloneqq \left\langle\hat{C}_{\ell,i}^{\gamma_{\rm E}\gamma_{\rm E},{\rm obs}}\hat{C}_{\ell,j}^{\gamma_{\rm E}\gamma_{\rm E},{\rm obs}}\right\rangle - \left\langle\hat{C}_{\ell,i}^{\gamma_{\rm E}\gamma_{\rm E},{\rm obs}}\right\rangle\left\langle\hat{C}_{\ell,j}^{\gamma_{\rm E}\gamma_{\rm E},{\rm obs}}\right\rangle \\ &= \frac{1}{\Omega_{\rm s}^2N_{{\rm mode},i}N_{{\rm mode},j}}\sum_{\boldsymbol{\ell}\in i}\sum_{\boldsymbol{\ell}'\in j}\left\langle\tilde{\gamma}_{\rm E}^{\rm obs}(\boldsymbol{\ell})\tilde{\gamma}_{\rm E}^{\rm obs}(-\boldsymbol{\ell})\tilde{\gamma}_{\rm E}^{\rm obs}(\boldsymbol{\ell}')\tilde{\gamma}_{\rm E}^{\rm obs}(-\boldsymbol{\ell}')\right\rangle \\ &\quad -C_{\ell,i}^{\gamma_{\rm E}\gamma_{\rm E},{\rm obs}}C_{\ell,j}^{\gamma_{\rm E}\gamma_{\rm E},{\rm obs}}.\end{aligned} \tag{4.54}$$

The accurate evaluation of this covariance requires knowledge of trispectrum of convergence and hence is challenging. Here I make a simplified assumption that convergence obeys random Gaussian

statistics for which the connected trispectrum is zero. In this case,

$$\begin{aligned}\left\langle \tilde{\gamma}_{\rm E}^{\rm obs}(\boldsymbol{\ell})\tilde{\gamma}_{\rm E}^{\rm obs}(-\boldsymbol{\ell})\tilde{\gamma}_{\rm E}^{\rm obs}(\boldsymbol{\ell}')\tilde{\gamma}_{\rm E}^{\rm obs}(-\boldsymbol{\ell}')\right\rangle &= \left\langle \tilde{\gamma}_{\rm E}^{\rm obs}(\boldsymbol{\ell})\tilde{\gamma}_{\rm E}^{\rm obs}(-\boldsymbol{\ell})\right\rangle \left\langle \tilde{\gamma}_{\rm E}^{\rm obs}(\boldsymbol{\ell}')\tilde{\gamma}_{\rm E}^{\rm obs}(-\boldsymbol{\ell}')\right\rangle \\ &+ \left\langle \tilde{\gamma}_{\rm E}^{\rm obs}(\boldsymbol{\ell})\tilde{\gamma}_{\rm E}^{\rm obs}(\boldsymbol{\ell}')\right\rangle \left\langle \tilde{\gamma}_{\rm E}^{\rm obs}(-\boldsymbol{\ell})\tilde{\gamma}_{\rm E}^{\rm obs}(-\boldsymbol{\ell}')\right\rangle \\ &+ \left\langle \tilde{\gamma}_{\rm E}^{\rm obs}(\boldsymbol{\ell})\tilde{\gamma}_{\rm E}^{\rm obs}(-\boldsymbol{\ell}')\right\rangle \left\langle \tilde{\gamma}_{\rm E}^{\rm obs}(\boldsymbol{\ell}')\tilde{\gamma}_{\rm E}^{\rm obs}(-\boldsymbol{\ell})\right\rangle ,\end{aligned} \tag{4.55}$$

and as a result covariance is simplified as

$$\left[{\rm Cov}(\hat{C}_\ell^{\gamma_{\rm E}\gamma_{\rm E}})\right]_{ij} = \frac{2\delta_{ij}}{N_{{\rm mode},i}}\left(C_{\ell,i}^{\gamma_{\rm E}\gamma_{\rm E},obs}\right)^2 = \frac{2\delta_{ij}}{N_{{\rm mode},i}}\left(C_{\ell,i}^{\gamma_{\rm E}\gamma_{\rm E}} + \frac{\sigma_{\epsilon/2}^2}{2\bar{n}}\right)^2 . \tag{4.56}$$

Although this expression of covariance ignores non-Gaussian effects and therefore is not accurate in general (see e.g., Takada & Jain, 2009; Takada & Hu, 2013, for effects of non-Gaussianity), it has several important implications. First, covariance is inversely proportional to $N_{{\rm mode},i}$, which is an increasing function of ℓ for a fixed ℓ-bin width. Hence measurements of power spectrum at low ℓ is noisy, due to a large cosmic variance. Second, it is also inversely proportional to the survey area $\Omega_{\rm s}$, which suggests that the signal-to-noise ratio of cosmic shear measurements is $\propto \sqrt{\Omega_{\rm s}}$. Third, the shot noise contributes to covariance, which tends to dominate at large ℓ. Fourth, covariance matrix is diagonal, which makes various calculations simpler.

5 Cosmology with cosmic shear

5.1 Behavior of power spectrum

In previous Section, I derived cosmic shear power spectrum (equation 4.41), which is essentially given by the integration of the matter power spectrum along the line-of-sight. On the other hand, from a large sample of distant galaxies with measurements of their ellipticities, one can in principle infer the E-mode shear power spectrum (equation 4.51). Therefore cosmological parameters can be constrained by searching for parameters that best reproduce the observed cosmic shear power spectrum. In order to understand what kind of constraints will be obtained, however, it is important to know behavior of cosmic shear power spectrum, including its sensitivity to various parameters.

Figure 6 shows an example of theoretical calculations of cosmic shear power spectrum in the current standard cosmological model. Since the standard cold dark model predicts large density fluctuations at small scales, cosmic shear also has a large power at large ℓ. The comparison with power spectrum computed from the linear matter power spectrum indicates that the nonlinear evolution of density fluctuations is indeed important for cosmic shear. At very large ℓ, measurements become very noisy due to large shot noise. Together with the fact that cosmic variance is large at small ℓ (see equation 4.56), for a typical case with $\bar{n} = 20$ arcmin^{-2} it is expected that constraints on cosmological parameters mainly come from $\ell \sim 10^3$.

It is worth noting that the power spectrum is relatively featureless. This is because any features in matter power spectrum, most notably baryon acoustic oscillations, are smeared out due to projection

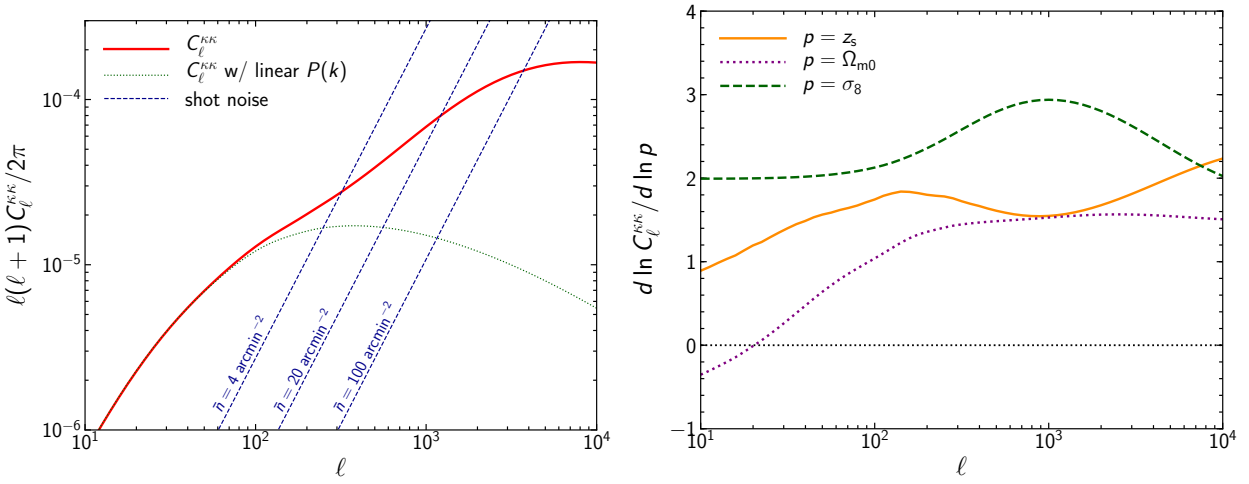

Figure 6: *Left:* The solid line shows cosmic shear power spectrum (equation 4.41) for the source redshift $z_\mathrm{s} = 1$ and assuming *Planck* 2018 best-fitting cosmological parameters (Planck Collaboration et al., 2018). The nonlinear matter power spectrum is computed using a revised *halofit* model (Takahashi et al., 2012). The dotted line shows cosmic shear power spectrum computed using the linear matter power spectrum. Dashed lines show the shot noise (second term of equation 4.49) with $\sigma_{\epsilon/2} = 0.4$ and three different source galaxy number densities $\bar{n}$. *Right:* Logarithmic derivatives of cosmic shear power spectrum for three important parameters, source redshift z_s (*solid*), matter density Ω_m0 (*dotted*), and the normalization of density fluctuations σ_8 (*dashed*), around the fiducial model shown in the left panel. When changing Ω_m0, $\Omega_{\Lambda 0}$ is also changed assuming the flat Universe.

that mixes different k-modes. Hence the main constraining power of cosmic shear power spectrum comes from its amplitude.

Figure 6 shows logarithmic derivatives of cosmic shear power spectrum. From this Figure, at $\ell = 1000$ it is found

$$C_{\ell=1000}^{\kappa\kappa} \propto z_\mathrm{s}^{1.5} \Omega_\mathrm{m0}^{1.5} \sigma_8^{2.9}, \tag{5.1}$$

around the fiducial model. This well explains the fact that cosmic shear constraints look a 'banana' shape in the Ω_m0-σ_8 plane. It is also found that to constrain $S_8 \coloneqq \sigma_8 (\Omega_\mathrm{m0}/0.3)^\alpha$ ($\alpha \approx 0.5$) accurately, say 5%, the average source redshift needs to be known at better than 10% accuracy. Since it is impractical to obtain spectroscopic redshifts for all the source galaxies used for weak gravitational lensing measurements, photometric redshifts are usually employed for estimating the average source redshift, and one challenge for cosmic shear cosmology is to obtain accurate photometric redshifts for such faint galaxies.

5.2 Cosmic shear tomography

Since weak gravitational lensing probes all the matter fluctuations along the line-of-sight, one cannot measure redshift evolution of density fluctuations from the analysis of a single galaxy sample. One

popular way to measure the redshift evolution is to split the galaxy sample into subsamples with different redshifts (Hu, 1999). Given the difference of the weight function for different source redshifts (see Figure 4), the redshift evolution is constrained to some extent. Since the weight function is broad, galaxies in different redshift bins usually have significant cross power spectrum.

5.3 Challenges

Just like other cosmological probes, there are many possible sources of systematic errors in cosmic shear analysis. These systematic errors must be kept under control in order to obtain accurate constraints. I do not go into detail here, but to guide future studies along this line I just list several topics that are worth investigating carefully.

- Shape measurements, in particular effects of blended (overlapping) galaxies.
- Photometric redshift accuracies, including accurate estimates of outliers, possibilities of clipping to remove galaxies with bad photometric redshifts.
- Improving theoretical predictions, in particular accurate estimates of impact of baryon physics (star formation, feedback, etc) on matter power spectrum.
- Intrinsic alignments of galaxies, their accurate modeling and how to mitigate their effects on cosmic shear.
- Measurement methods, such as two-point correlation functions versus power spectrum, their complementary, etc. Analysis in curved sky.
- Limitations of various approximations, such as locally flat sky, Limber, and Born approximations (may be important in future surveys).
- Accurate and fast calculation of covariance, including effects of super-survey modes.
- Model predictions in different cosmological models, such as modified gravity theories.

A Calculations in conformal Newtonian gauge

A.1 Metric

I summarize various calculations for the following spacetime metric

$$ds^2 = g_{\mu\nu}dx^\mu dx^\nu \coloneqq -\left(1+\frac{2\Phi}{c^2}\right)c^2dt^2 + a^2\left(1-\frac{2\Psi}{c^2}\right)\gamma_{ij}dx^i dx^j \qquad (\mu,\nu=0,1,2,3), \tag{A.1}$$

where

$$\gamma_{ij}dx^i dx^j \coloneqq d\chi^2 + f_K^2(\chi)\left(d\theta^2+\sin^2\theta d\phi^2\right) \qquad (i,j=1,2,3), \tag{A.2}$$

and $f_K(\chi)$ is defined by equation (1.2). The covariant metric is defined such that it satisfies $g^{\mu\alpha}g_{\alpha\nu} = \delta^\mu{}_\nu$, where $\delta^\mu{}_\nu$ denotes the Kronecker delta. Below all the calculations will be done up to the first order in Φ and Ψ. I use the Einstein summation convention, and also comma derivative i.e., $f_{,\mu} \coloneqq \partial f/\partial x^\mu$.

A.2 Christoffel symbols

Christoffel symbols are defined by

$$\Gamma^{\alpha}{}_{\mu\nu} \coloneqq \frac{1}{2} g^{\alpha\beta} \left(g_{\nu\beta,\mu} + g_{\mu\beta,\nu} - g_{\mu\nu,\beta} \right). \tag{A.3}$$

Their explicit expressions for the metric (A.1) are

$$\Gamma^{0}{}_{00} = \frac{\dot{\Phi}}{c^3}, \quad \Gamma^{0}{}_{0i} = \Gamma^{0}{}_{i0} = \frac{\Phi_{,i}}{c^2}, \quad \Gamma^{0}{}_{ij} = \frac{a^2}{c} \gamma_{ij} \left[H \left(1 - \frac{2\Phi}{c^2} - \frac{2\Psi}{c^2} \right) - \frac{\dot{\Psi}}{c^2} \right], \tag{A.4}$$

$$\Gamma^{i}{}_{00} = \frac{\gamma^{il}}{a^2} \frac{\Phi_{,l}}{c^2}, \quad \Gamma^{i}{}_{0j} = \Gamma^{i}{}_{j0} = \frac{\delta^{i}{}_{j}}{c} \left(H - \frac{\dot{\Psi}}{c^2} \right), \tag{A.5}$$

$$\Gamma^{i}{}_{jk} = {}^{(3)}\Gamma^{i}{}_{jk} + \frac{1}{c^2} \left(\gamma_{jk} \gamma^{il} \Psi_{,l} - \delta^{i}{}_{j} \Psi_{,k} - \delta^{i}{}_{k} \Psi_{,j} \right), \tag{A.6}$$

where ${}^{(3)}\Gamma^{i}{}_{jk}$ denote Christoffel symbols computed from γ_{ij} defined by equation (A.2)

$${}^{(3)}\Gamma^{i}{}_{jk} \coloneqq \frac{1}{2} \gamma^{il} \left(\gamma_{kl,j} + \gamma_{jl,k} - \gamma_{jk,l} \right). \tag{A.7}$$

A.3 Ricci curvature

The Ricci curvature tensor is defined by

$$R_{\mu\nu} \coloneqq \Gamma^{\alpha}{}_{\nu\mu,\alpha} - \Gamma^{\alpha}{}_{\alpha\mu,\nu} + \Gamma^{\alpha}{}_{\alpha\beta} \Gamma^{\beta}{}_{\nu\mu} - \Gamma^{\alpha}{}_{\nu\beta} \Gamma^{\beta}{}_{\alpha\mu}. \tag{A.8}$$

Explicit expressions for the metric (A.1) are

$$R_{00} = -\frac{3\ddot{a}}{c^2 a} + \frac{3\ddot{\Psi}}{c^4} + \frac{3H\dot{\Phi}}{c^4} + \frac{6H\dot{\Psi}}{c^4} + \frac{{}^{(3)}\Delta\Phi}{c^2 a^2}, \tag{A.9}$$

$$R_{0i} = \frac{2\dot{\Psi}_{,i}}{c^3} + \frac{2H\Phi_{,i}}{c^3}, \tag{A.10}$$

$$\begin{aligned} R_{ij} \;=\; & {}^{(3)}R_{ij} - \frac{\Phi_{|ij}}{c^2} + \frac{\Psi_{|ij}}{c^2} \\ & + \left[\left(\frac{2a^2H^2}{c^2} + \frac{a\ddot{a}}{c^2} \right) \left(1 - \frac{2\Phi}{c^2} - \frac{2\Psi}{c^2} \right) - \frac{a^2\ddot{\Psi}}{c^4} - \frac{a^2H\dot{\Phi}}{c^4} - 6\frac{a^2H\dot{\Psi}}{c^4} + \frac{{}^{(3)}\Delta\Psi}{c^2} \right] \gamma_{ij}, \end{aligned} \tag{A.11}$$

where ${}^{(3)}R_{ij}$ is the Ricci curvature tensor computed from γ_{ij}. For γ_{ij} defined by equation (A.2), ${}^{(3)}R_{ij}$ is given by

$${}^{(3)}R_{ij} = 2K\gamma_{ij}. \tag{A.12}$$

In the expressions of the Ricci curvature tensor above I also used the three-dimensional Laplace operator defined by

$$ {}^{(3)}\Delta f \coloneqq \frac{1}{\sqrt{|\gamma|}}\frac{\partial}{\partial x^j}\left(\sqrt{|\gamma|}\gamma^{ij}\frac{\partial f}{\partial x^i}\right) = \gamma^{ij}f_{,ij} + \gamma^{ij}{}_{,j}f_{,i} + {}^{(3)}\Gamma^k{}_{kj}\gamma^{ij}f_{,i}, \tag{A.13} $$

$$ {}^{(3)}\Gamma^k{}_{kj} = \frac{1}{\sqrt{|\gamma|}}\frac{\partial}{\partial x^j}\sqrt{|\gamma|}, \tag{A.14} $$

where γ denotes the determinant of γ_{ij}. Also the vertical bar represents the covariant derivative with respect to γ_{ij} i.e.,

$$ f_{|ij} \coloneqq f_{,ij} - {}^{(3)}\Gamma^l{}_{ij}f_{,l}. \tag{A.15} $$

With this notation the Laplace operator is described as ${}^{(3)}\Delta f = \gamma^{ij}f_{|ij} = f^{|i}{}_{|i}$.

A.4 Scalar curvature

By contracting the Ricci tensor I obtain the scalar curvature

$$ \begin{aligned} R &\coloneqq g^{\mu\nu}R_{\mu\nu} \\ &= \frac{6}{c^2}\left(H^2 + \frac{\ddot{a}}{a} + \frac{c^2K}{a^2}\right) - \frac{12}{c^2}\left(H^2 + \frac{\ddot{a}}{a}\right)\frac{\Phi}{c^2} + \frac{12\Psi K}{c^2a^2} \\ &\quad -\frac{6\ddot{\Psi}}{c^4} - \frac{6H\dot{\Phi}}{c^4} - \frac{24H\dot{\Psi}}{c^4} - \frac{2{}^{(3)}\Delta\Phi}{c^2a^2} + \frac{4{}^{(3)}\Delta\Psi}{c^2a^2}. \end{aligned} \tag{A.16} $$

A.5 Einstein tensor

The Einstein tensor is defined by

$$ G^\mu{}_\nu \coloneqq g^{\mu\alpha}R_{\alpha\nu} - \frac{1}{2}\delta^\mu{}_\nu R. \tag{A.17} $$

Their explicit expressions are

$$ G^0{}_0 = -\frac{3}{c^2}\left(H^2 + \frac{c^2K}{a^2}\right) + \frac{6H^2\Phi}{c^4} - \frac{6\Psi K}{c^2a^2} + \frac{6H\dot{\Psi}}{c^4} - \frac{2{}^{(3)}\Delta\Psi}{c^2a^2}, \tag{A.18} $$

$$ G^0{}_i = -\frac{2\dot{\Psi}_{,i}}{c^3} - \frac{2H\Phi_{,i}}{c^3}, \tag{A.19} $$

$$ \begin{aligned} G^i{}_j &= \left[-\frac{1}{c^2}\left(H^2 + 2\frac{\ddot{a}}{a} + \frac{c^2K}{a^2}\right) + \frac{2}{c^2}\left(H^2 + 2\frac{\ddot{a}}{a}\right)\frac{\Phi}{c^2} - \frac{2\Psi K}{c^2a^2}\right. \\ &\quad \left. + \frac{2\ddot{\Psi}}{c^4} + \frac{2H\dot{\Phi}}{c^4} + \frac{6H\dot{\Psi}}{c^4} + \frac{{}^{(3)}\Delta\Phi}{c^2a^2} - \frac{{}^{(3)}\Delta\Psi}{c^2a^2}\right]\delta^i{}_j - \frac{1}{c^2a^2}\left(\Phi^{|i}{}_{|j} - \Psi^{|i}{}_{|j}\right). \end{aligned} \tag{A.20} $$

A.6 Einstein equation

The perturbed stress-energy tensor is given by

$$T^0{}_0 = -\sum_\alpha (\rho_\alpha + \delta\rho_\alpha), \tag{A.21}$$

$$T^0{}_i = \sum_\alpha (\rho_\alpha + p_\alpha)\frac{a v_{\alpha i}}{c}, \tag{A.22}$$

$$T^i{}_j = \sum_\alpha (p_\alpha + \delta p_\alpha)\delta^i{}_j + \sigma_\alpha{}^i{}_j, \tag{A.23}$$

where ρ_α and p_α are background quantities and $\delta\rho_\alpha$, $v_{\alpha i}$, δp_α, and $\sigma_\alpha{}^i{}_j$ are perturbations. $\sigma_\alpha{}^i{}_j$ is an anisotropic stress tensor that is defined to be traceless i.e.,

$$\sigma_\alpha{}^i{}_i = 0. \tag{A.24}$$

It is straightforward to see that the zero-th order Einstein equation recovers equation (1.4) and (1.5). On the other hand the first order equations are given by

$$-\frac{3H^2\Phi}{c^2} + \frac{3\Psi K}{a^2} - \frac{3H\dot\Psi}{c^2} + \frac{{}^{(3)}\Delta\Psi}{a^2} = \frac{4\pi G}{c^2}\sum_\alpha \delta\rho_\alpha, \tag{A.25}$$

$$-\dot\Psi_{,i} - H\Phi_{,i} = \frac{4\pi G}{c^2}\sum_\alpha (\rho_\alpha + p_\alpha) a v_{\alpha i}, \tag{A.26}$$

$$\left[\left(H^2 + 2\frac{\ddot a}{a}\right)\frac{\Phi}{c^2} - \frac{\Psi K}{2a^2} + \frac{\ddot\Psi}{c^2} + \frac{H\dot\Phi}{c^2} + \frac{3H\dot\Psi}{c^2} + \frac{{}^{(3)}\Delta\Phi - {}^{(3)}\Delta\Psi}{3a^2}\right] = \frac{4\pi G}{c^2}\sum_\alpha \delta p_\alpha, \tag{A.27}$$

$$\frac{1}{3c^2a^2}\left({}^{(3)}\Delta\Phi - {}^{(3)}\Delta\Psi\right)\delta^i{}_j - \frac{1}{c^2a^2}\left(\Phi^{|i}{}_{|j} - \Psi^{|i}{}_{|j}\right) = \frac{8\pi G}{c^4}\sum_\alpha \sigma_\alpha{}^i{}_j, \tag{A.28}$$

where trace and traceless parts of the (ij) component of the Einstein equation are separated.

A.7 Sub-horizon limit

Equations (A.25)–(A.28) can be used to derive evolution of fluctuations at various scales. In this lecture, however, I mostly focus on fluctuations at the sub-horizon scale in the late Universe, where $\partial/\partial x \gg aH/c$, the dominant component of fluctuations is matter ($\alpha = \mathrm{m}$), and there is no source of anisotropic stress ($\sigma_\alpha{}^i{}_j = 0$). In addition at the small scale the effect of curvature can be ignored i.e., ${}^{(3)}\Delta \gg K$. In this case, the evolution equations are simplified as

$${}^{(3)}\Delta\Phi = \frac{4\pi G a^2}{c^2}\delta\rho_{\mathrm{m}}, \tag{A.29}$$

$$-\dot\Phi_{,i} - H\Phi_{,i} = \frac{4\pi G}{c^2}\rho_{\mathrm{m}} a v_{\mathrm{m}i}, \tag{A.30}$$

$$\ddot{\Phi} + 4H\dot{\Phi} + \left(H^2 + 2\frac{\ddot{a}}{a}\right)\Phi = 0, \tag{A.31}$$

$$\Phi - \Psi = 0, \tag{A.32}$$

where I replaced Ψ to Φ given equation (A.32). I now define the density perturbation

$$\delta_{\rm m} \coloneqq \frac{\delta\rho_{\rm m}}{\rho_{\rm m}}. \tag{A.33}$$

Equation (A.29) is rewritten as

$${}^{(3)}\Delta\Phi = \frac{4\pi G a^2 \rho_{\rm m}}{c^2}\delta_{\rm m}, \tag{A.34}$$

which is called the Poisson equation. By taking the divergence of equation (A.30) and combine it with equation (A.29) and $\rho_{\rm m} \propto a^{-3}$, it is straightforward to show

$${}^{(3)}\nabla \cdot \boldsymbol{v} = v_{{\rm m}i}{}^{,i} = -a\dot{\delta}_{\rm m}. \tag{A.35}$$

From equations (A.30) and (A.31) it is also shown

$$\left(\frac{\partial}{\partial t} + H\right) v_{{\rm m}i}{}^{,i} = -\frac{{}^{(3)}\Delta\Phi}{a}. \tag{A.36}$$

Combining equations (A.35) and (A.36), the evolution equation for the density perturbation is obtained as

$$\ddot{\delta}_{\rm m} + 2H\dot{\delta}_{\rm m} - \frac{4\pi G\rho_{\rm m}}{c^2}\delta_{\rm m} = 0. \tag{A.37}$$

This is an important equation that governs the growth of structure in the late Universe. It has the following two solutions

$$\text{growing mode}: \qquad D_+ \propto H\int_0^a \frac{da}{a^3H^3}, \tag{A.38}$$

$$\text{decaying mode}: \qquad D_- \propto H. \tag{A.39}$$

In cosmological analyses only the growing mode is important. For the simplest Einstein–de Sitter Universe ($\Omega_{\rm m0} = 1$, $\Omega_{\Lambda 0} = 0$), from equation (1.14) it is easily found $D_+(a) \propto a$ i.e., structure grows linearly with the scale factor. In the current standard cosmology with a signification contribution of cosmological constant, however, the friction term $2H\dot{\delta}_{\rm m}$ is larger and hence the growth of structure becomes slower than a. Figure 7 clearly shows that the growth becomes slower than a in the late Universe when cosmological constant contributes to the expansion rate of the Universe, and when $\Omega_{\Lambda 0}$ is larger the suppression of the growth is stronger.

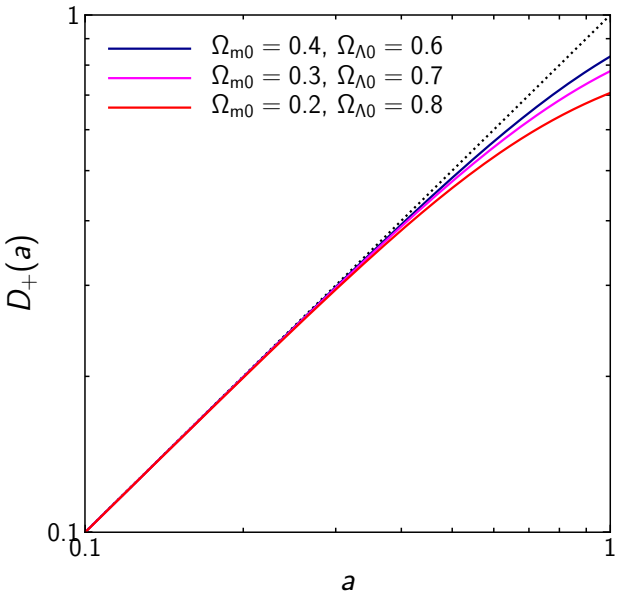

Figure 7: Linear growth rate D_+ (equation A.38) as a function of scale factor a for three different cosmological parameter sets. Here the normalization is determined so as to satisfy $D_+(a)/a \approx 1$ at $a \ll 1$. The dotted line shows $D_+ \propto a$, which is the solution in the Einstein–de Sitter Universe ($\Omega_{\rm m0} = 1$, $\Omega_{\Lambda 0} = 0$).

A.8 Decomposition into radial and angular parts

For calculating gravitational lensing effects, it is useful to decompose the spatial metric γ_{ij} into radial and angular parts. Specifically, I rewrite equation (A.2) as

$$\gamma_{ij}dx^i dx^j = d\chi^2 + f_K^2(\chi)\omega_{ab}dx^a dx^b \qquad (a, b = 2, 3), \tag{A.40}$$

$$\omega_{ab}dx^a dx^b \coloneqq d\theta^2 + \sin^2\theta d\phi^2. \tag{A.41}$$

Explicit expressions for Christoffel symbols ${}^{(3)}\Gamma^i{}_{jk}$ (equation A.7) are

$${}^{(3)}\Gamma^1{}_{11} = {}^{(3)}\Gamma^1{}_{1a} = {}^{(3)}\Gamma^1{}_{a1} = {}^{(3)}\Gamma^a{}_{11} = 0, \quad {}^{(3)}\Gamma^1{}_{ab} = -f_K(\chi)f_K'(\chi)\omega_{ab}, \tag{A.42}$$

$${}^{(3)}\Gamma^a{}_{1b} = {}^{(3)}\Gamma^a{}_{b1} = \frac{f_K'(\chi)}{f_K(\chi)}\delta^a{}_b, \quad {}^{(3)}\Gamma^a{}_{bc} = {}^{(2)}\Gamma^a{}_{bc}, \tag{A.43}$$

where ${}^{(2)}\Gamma^a{}_{bc}$ are Christoffel symbols computed from ω_{ab}

$${}^{(2)}\Gamma^a{}_{bc} \coloneqq \frac{1}{2}\omega^{ad}\left(\omega_{cd,b} + \omega_{bd,c} - \omega_{bc,d}\right). \tag{A.44}$$

References

Born, M. 1926, Zeitschrift fur Physik, 38, 803

Dodelson, S. 2003, Modern cosmology

Event Horizon Telescope Collaboration, Akiyama, K., Alberdi, A., et al. 2019, ApJ, 875, L1

Hikage, C., Oguri, M., Hamana, T., et al. 2019, PASJ, 71, 43

Hu, W. 1999, ApJ, 522, L21

Jain, B., & Khoury, J. 2010, Annals of Physics, 325, 1479

Kaiser, N. 1992, ApJ, 388, 272

Krause, E., & Hirata, C. M. 2010, A&A, 523, A28

Limber, D. N. 1954, ApJ, 119, 655

Loverde, M., & Afshordi, N. 2008, Phys. Rev. D, 78, 123506

Matsubara, T. 2010, Modern Cosmology (in Japanese)

Mo, H., van den Bosch, F. C., & White, S. 2010, Galaxy Formation and Evolution

Planck Collaboration, Aghanim, N., Akrami, Y., et al. 2018, arXiv e-prints, arXiv:1807.06209

Schneider, P. 1985, A&A, 143, 413

Takada, M., & Hu, W. 2013, Phys. Rev. D, 87, 123504

Takada, M., & Jain, B. 2009, MNRAS, 395, 2065

Takahashi, R., Sato, M., Nishimichi, T., Taruya, A., & Oguri, M. 2012, ApJ, 761, 152

Troxel, M. A., & Ishak, M. 2015, Phys. Rep., 558, 1

Weinberg, S. 2008, Cosmology